ISSN 0280-5316
ISRN LUTFD2/TFRT--5697--SE

Optimal Vehicle Dynamics – Yaw Rate and Side Slip Angle Control Using 4-Wheel Steering

Nenad Lazic

Department of Automatic Control
Lund Institute of Technology
October 2002

Department of Automatic Control
Lund Institute of Technology
Box 118
SE-221 00 Lund Sweden

Document name
MASTER THESIS

Date of issue
October 2002

Document Number
ISRN LUTFD2/TFRT--5697--SE

Author(s)
Nenad Lasic

Supervisor
Anders Rantzer, LTH
Jens Kalkkuhl DaimlerChrysler AG, Stuttgart

Sponsoring organization

Title and subtitle
Optimal Vehicle Dynamics – Yaw Rate and Side Slip Angle Control Using 4-Wheel Steering.
(Optimal fordonsdynamik vid 4-hjulsstyrning).

Abstract
The development of steer-by-wire involves an increased amount of possibilities for control in future cars. For example, the experimental vehicle available has both front and rear wheel steering. This enables a simultaneous multivariable control of both the yaw rate and the side slip angle. The today existing control approach is designed in the time domain and it has a decoupled control structure, where the yaw rate is controlled by the front wheel steering angle, and the side slip angle is controlled by the rear wheel steering angle. With this approach there are some major difficulties, such as constraint handling and lack of robustness to plant uncertainties, to time delays and to actuator or sensor failure. To solve these problems, a multivariable control scheduling system can be used that has already been applied to robotics, satellite attitude control and ship control but is a novelty for the field of automotive control. It is a coupling control approach, based on Individual Channel Design in the frequency domain, ICD, and considers the internal cross-coupling of the plant. It has been shown that meeting the requirements is not trivial, and a tradeoff has to be done between high performance and entirely meeting the specifications. However, the design shows a considerable degree of both robustness and integrity, which has been verified in theory as well as in simulations, but has to be further checked in real experiments.

Keywords

Classification system and/or index terms (if any)

Supplementary bibliographical information

ISSN and key title
0280-5316

ISBN

Language
English

Number of pages
90

Recipient's notes

Security classification

Optimal Vehicle Dynamics - Yaw Rate and Side Slip Angle Control Using 4-Wheel Steering

Nenad Lazic

October 23, 2002

Contents

Acknowledgements

This thesis was done in cooperation between DaimlerChrysler AG, Stuttgart, and the Department of Automatic Control, Lund Institute of Technology. It has been carried out at the Department of Driver Assistant Systems, DaimlerChrysler, in Esslingen, just outside Stuttgart, from March to September 2002.

I am grateful to all the people at the department in Esslingen. Especially I would like to thank Dr. Jens Kalkkuhl for his great supervising and support throughout my work. I also would like to thank Prof. Anders Rantzer for giving me the opportunity to do this thesis and for giving me valuable comments on the report.

Lund, October 2002
Nenad Lazic

1 Introduction

1.1 Problem Formulation

Today's cars are becoming more and more sophisticated. They contain more electrical hardware components and less mechanical and hydraulic ones. Examples of this are the actuators used for control such as in brake-by-wire, steer-by-wire and active suspension. In future cars there might be a very large number of possible configurations for these actuators. This means that forces and torque for control action can be applied in many different ways. What we want is to optimally employ these actuators such that

- control is achieved with minimum control action
- the solution is robust to plant uncertainties, and a failure of one actuator can be compensated by the remaining ones
- the controller can be adapted to any specific actuator configuration

To achieve all three objectives, a multivariable control scheduling system has to be used that has already been applied to robotics, satellite attitude control and ship control but is a novelty for the field of automotive control. It requires the solution of problems unique to automotive control such as

- handling uncertain nonlinear tyre forces
- time varying constraints on the maximum available tyre forces due to changing road conditions

Using existing modelled vehicle dynamics, reference yaw rate and side slip angle are generated from a driver command. With proper model matching, and considering disturbances and uncertainties, control commands should be given such that the reference is followed.

In this work 4 wheel steering (front and rear axle) is used for control, with yaw rate and side slip angle as outputs from the car, and front and rear wheel steering angles as the input to the car. The problem is to control the yaw rate and side slip angle simultaneously (normally, the side slip angle has to be kept under a certain threshold), and at the same time fulfil the specifications that are set up for the control system.

The internal structure of the system involves a certain degree of cross-coupling between inputs and outputs. An approach with a decoupled controller structure, as well as a model based state space design in the time domain, where one controller is used for yaw rate and another for side slip angle, constructed independently of each other, already exists. The front

wheel steering angle is generated using both feedforward and feedback, and for the rear wheel steering angle only feedforward is used. This decoupling approach has some major disadvantages. One is the lack of robustness, both to plant uncertainties and time delays. The limitations in constraint handling are another disadvantage.

By also taking the dependency between yaw rate and side slip angle control into account, and using a coupling approach, a more robust solution can be obtained that meets the theory and specifications in a better way. The intention is to use feedforward and feedback for both rear and front wheel steering. However, feedback design will be the central point.

1.2 Thesis Outline

This work consists of three main parts. The first part, system modelling, problem specification and survey of different design strategies, is discussed in chapter 2 to chapter 4. In chapter 2 the fundamental concepts of vehicle dynamics are explained. The general ideas and specifications of the multivariable controller design are discussed in chapter 3. Some ideas about feedforward will be presented, but focus will be put on feedback design. The feedback design approach chosen for this work, *Individual Channel Design*, is explained in chapter 4. Beyond that, a rough structure for the controller will be discussed in the chapter.

The second part is the controller design. This will be described in chapter 5. The software environment used for the design is Matlab, and in particular the SISO root-locus design tool in Matlab.

Simulations and experimental results are the third part of this work. The simulations will be carried out in Matlab Simulink. A complete car model, containing the same dynamics as a real car, will be used to verify the performance and robustness of the controller. The simulation results are discussed in chapter 6. The most important parts of the Matlab code used during the design are given in the Appendix.

2 The Car Model

When modelling car dynamics different co-ordinate systems can be used depending on the physical quantity considered.

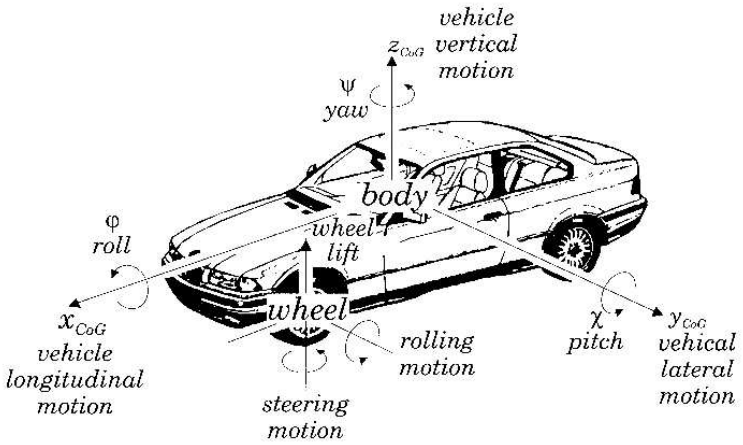

Figure 2.1: The different degrees of freedom of the vehicle.

- *The center of gravity co-ordinate system* (figure 2.2) has its origin at the vehicle center of gravity and is of the most importance. This co-ordinate system is used as the reference for all movements of the vehicle body.
- *The fixed inertial system* (figure 2.3) is the only co-ordinate system that doesn't move during travel but is instead used as a reference for the position of the vehicle, i.e the center of gravity co-ordinate system.
- *The wheel co-ordinate system* (figure 2.4) can be different for each individual wheel but differs normally only between front and rear axle.

Figure 2.1 shows the six degrees of freedom of the vehicle as well as the center of gravity coordinate system.

The most important variables and quantities for the co-ordinate systems are summarized in table 2.1 and they will all be explained at some point in the chapter.

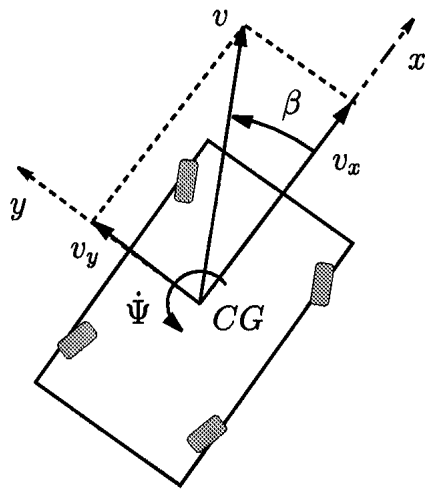

Figure 2.2: The CoG co-ordinate system and its main quantities.

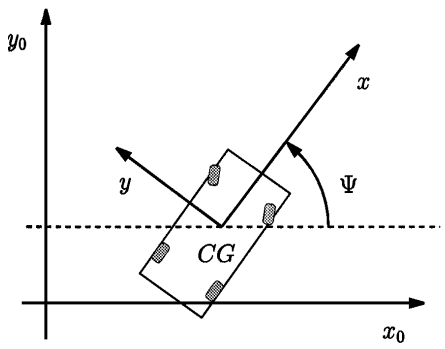

Figure 2.3: The CoG co-ordinate system in relation to the inertial.

2.1 Wheel Model

The location of the wheel ground contact point (marked by P in figure 2.4) normally differs from the origin of the wheel co-ordinate system. Its exact location depends on the steering mechanism, the vertical normal force distribution of the vehicle, the tyre stiffness and is described by the casters n_u and n_s. The frictional forces (S and U in figure 2.4) that act on the wheel in the contact point determine the behaviour of the vehicle. The dynamic characteristics of these forces are nonlinear with respect to the *wheel slip* (see

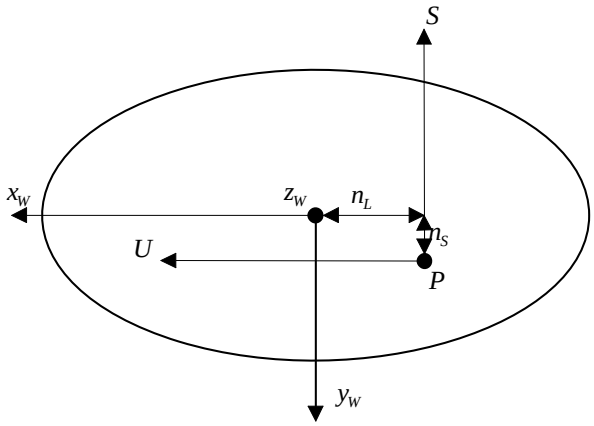

Figure 2.4: The wheel co-ordinate system. Road surface contact area viewed from above.

Table 2.1: Co-ordinate system variables

$x_{CoG}, y_{CoG}, z_{CoG}$	Axis for the center of gravity co-ordinate system
x_W, y_W, z_W	Axis for the wheel co-ordinate system
x_{In}, y_{In}, z_{In}	Axis for the inertial co-ordinate system
ψ	Yaw angle (rotation about z_{CoG})
α	Tyre side slip angle (angle between x_W and v_W, the wheel ground contact point velocity)
δ	Wheel steering angle
β	Vehicle body side slip angle (angle between x_{CoG} and v_{CoG}, the vehicle velocity)
$S_{f/r}$	Lateral wheel ground contact force (acting in the direction of y_W)
$U_{f/r}$	Longitudinal wheel ground contact force (acting in the direction of x_W)
v_x	The forward velocity, in the direction of x_{CoG}
v_y	The lateral velocity, in the direction of y_{CoG}
v	The resulting velocity. Geometrical sum of v_x and v_y
C_s, C_u	Tyre stiffness in the direction of y_W and x_W
λ_s, λ_u	Wheel slip in the direction of y_W and x_W

figure 2.5), which is defined as

$$\lambda_u = \frac{\omega_{wheel} \cdot r_{wheel} - v_u}{v_r} \tag{2.1}$$

$$\lambda_s = \sin\alpha \approx \alpha \tag{2.2}$$

$$\lambda_r = \sqrt{\lambda_u^2 + \lambda_s^2} \tag{2.3}$$

where v_r is the geometrical sum of the longitudinal and lateral wheel velocity components v_u and v_s. The tyre force saturates when a certain wheel slip is reached. The definition of the wheel slip varies in the literature. Here it

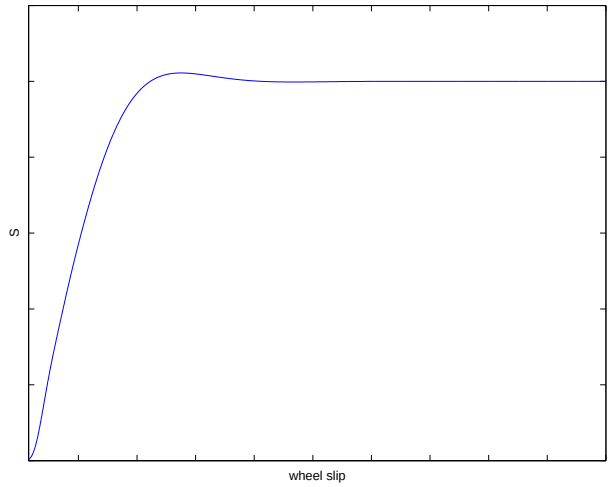

Figure 2.5: Lateral tyre force S vs. wheel slip λ_s.

is defined in the longitudinal and lateral direction of the wheel co-ordinate system. The presence of a lateral wheel slip λ_s causes the velocity vector of the wheel to have a direction different from x_W. The resulting angle is called *tyre side slip angle* (figure 2.6) and is defined as

$$\alpha_f = \delta_f + \beta_f = \delta_f + \beta - \frac{l_f}{v_x}\dot{\psi} \tag{2.4a}$$

$$\alpha_r = \delta_r + \beta_r = \delta_r + \beta + \frac{l_r}{v_x}\dot{\psi} \tag{2.4b}$$

where β is the side slip angle of the entire vehicle body (angle between vehicle center of gravity velocity vector and x_{CoG}) and δ is the steering angle. β_f and β_r are transformations of the side slip angle to, respectively, the front and the rear axle. $\dot{\psi}$ (yaw rate) is the rotational speed around z_{CoG}. The presence of the wheel casters will introduce a slight change in the wheel steering angle

$$\delta = \delta^* - \frac{n_s}{C_L}S \tag{2.5}$$

where δ^* is the original angle given by the steering mechanism and C_L is an elasticity constant. If we use a linearised static wheel lateral force $S = C_s\lambda_s \approx C_s\alpha$ (linear part in figure 2.5), where C_s is the lateral tyre cornering

stiffness, and combine it with equation (2.5), the resulting equation for the tyre force S will be

$$S = \frac{C_s}{1 + \frac{C_s}{C_L} n_s} (\delta^* + \beta) = C_s^* \alpha^* \tag{2.6}$$

The virtual tyre stiffness C_s^* is reduced in comparison to C_s.

The dynamic tyre characteristics can be modelled linearly or nonlinearly. The linear approach simplifies the design but is of limited use:

$$\overline{S} = \left. \frac{\partial S}{\partial \lambda_s} \right|_{\lambda_s = \lambda_u = 0} \cdot \lambda_s = C_s \lambda_s \approx C_s \alpha \tag{2.7}$$

$$\overline{U} = \left. \frac{\partial U}{\partial \lambda_u} \right|_{\lambda_s = \lambda_u = 0} \cdot \lambda_u = C_u \lambda_u \tag{2.8}$$

The complete nonlinear model is [Niethammer]

$$\overline{S} = \begin{cases} \frac{C_s \lambda_s}{(\xi_s - 1)^2 + C_s^* \xi_s} & \xi_s \leq 1, \\ \frac{\lambda_s}{\lambda_r} \mu_s F_z & \xi_s > 1 \end{cases} \tag{2.9}$$

$$\overline{U} = \begin{cases} \frac{C_u \lambda_u}{(\xi_u - 1)^2 + C_u^* \xi_u} & \xi_u \leq 1, \\ \frac{\lambda_u}{\lambda_r} \mu_u F_z & \xi_u > 1 \end{cases} \tag{2.10}$$

with the following definitions of the normalised wheel slip

$$\xi_s = \frac{\lambda_r}{\lambda_{Smax}} \tag{2.11}$$

$$\xi_u = \frac{\lambda_r}{\lambda_{Umax}} \tag{2.12}$$

2.2 The One-track Bicycle Model

As a base for the controller design a linear one-track bicycle model is used (figure 2.6). This simple model considers front and rear wheel steering as well as actuator dynamics. It is not very well purposed for simulation, but for controller design it should be sufficient.

To obtain information about the behaviour of the system, in other words the transfer function $G(s)$, a state space representation is made, with the yaw rate, $\dot{\psi}$, and the side slip angle at the rear axle, β_r, as outputs and front and rear wheel steering angles, (δ_f, δ_r), as inputs to the process. The input, output and state vectors are

$$u = \begin{pmatrix} u_1 \\ u_2 \end{pmatrix} = \begin{pmatrix} \delta_f \\ \delta_r \end{pmatrix} \tag{2.13}$$

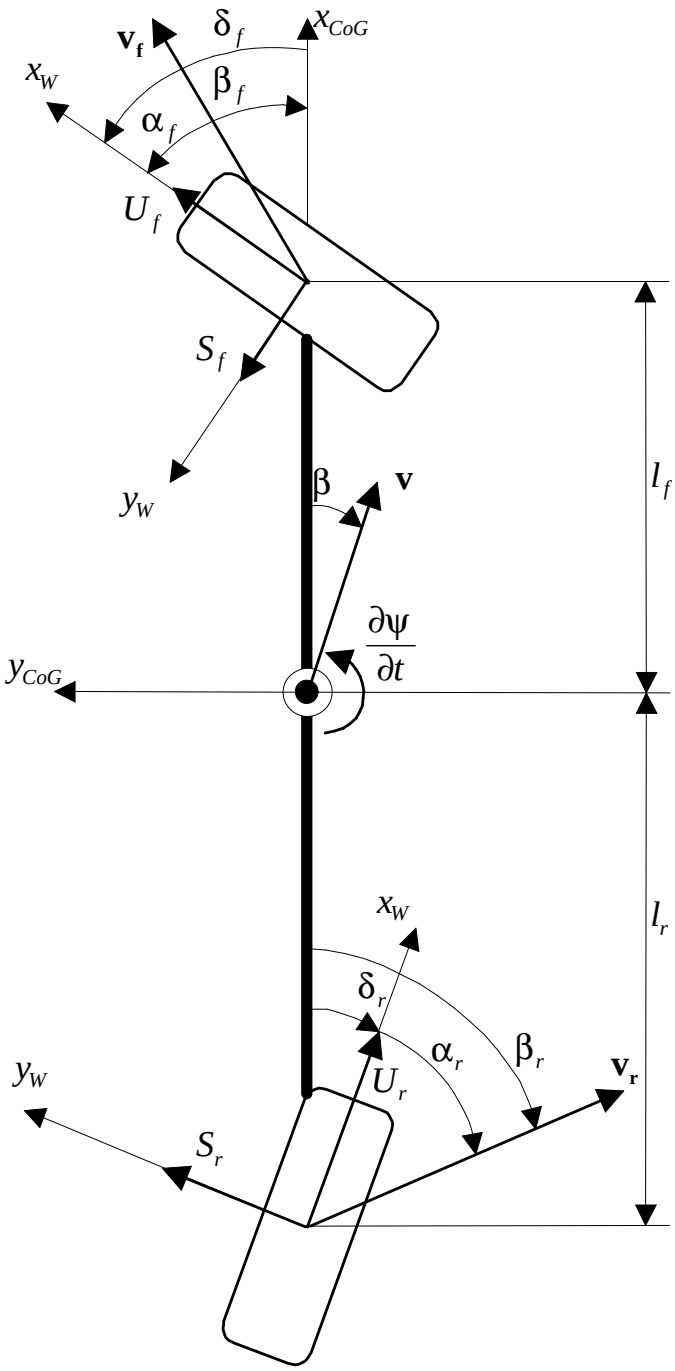

Figure 2.6: The one-track bicycle model.

$$y = \begin{pmatrix} y_1 \\ y_2 \end{pmatrix} = \begin{pmatrix} \dot{\psi} \\ \beta_r \end{pmatrix} \tag{2.14}$$

$$x = \begin{pmatrix} \dot{\psi} \\ \beta_r \\ S_f \\ S_r \end{pmatrix} \tag{2.15}$$

The force equations of the vehicle are

$$\begin{aligned} ma_x &= F_{Xf} + F_{Xr} = m\left(\dot{v}_x - v_y\dot{\psi}\right) \\ ma_y &= F_{Yf} + F_{Yr} = m\left(\dot{v}_y + v_x\dot{\psi}\right) \end{aligned} \tag{2.16}$$

where F_{Xf} and F_{Xr} act in the vehicle direction and F_{Yf} and F_{Yr} are lateral forces. The moment equilibrium around the center of mass leads to the differential equation

$$I_{zz}\ddot{\psi} = F_{Yf}l_f - F_{Yr}l_r \tag{2.17}$$

where the forces can be rewritten as

$$\begin{aligned} F_{Xf} &= U_f\cos\delta_f - S_f\sin\delta_f \\ F_{Xr} &= U_r\cos\delta_r - S_r\sin\delta_r \\ F_{Yf} &= U_f\sin\delta_f + S_f\cos\delta_f \\ F_{Yr} &= U_r\sin\delta_r + S_r\cos\delta_r \end{aligned} \tag{2.18}$$

By assuming small front and rear wheel steering angles, a linearisation can be made:

$$\begin{aligned} \cos\delta_f = \cos\delta_r &= 1 \\ \sin\delta_f &= \delta_f \\ \sin\delta_r &= \delta_r \\ U_f = U_r &= 0 \end{aligned} \tag{2.19}$$

Combining equation (2.18) with the equations (2.17) and (2.16) gives

$$\ddot{\psi} = \frac{1}{I_{zz}}\left(l_fS_f - l_rS_r\right) \tag{2.20}$$

$$\dot{v}_y = -v_x\dot{\psi} + \frac{S_f + S_r}{m} \tag{2.21}$$

The side slip angle β is defined as

$$\beta = \arctan\left(-\frac{v_y}{v_x}\right) \approx -\frac{v_y}{v_x} \tag{2.22}$$

Assuming a constant v_x, and combining (2.21) with (2.22), gives the differential equation for the side slip angle

$$\dot{\beta} = \dot{\psi} - \frac{S_f + S_r}{m v_x} \tag{2.23}$$

With

$$\beta_r = \beta + \frac{I_{zz}}{l_f m v_x}\dot{\psi} \tag{2.24}$$

the side slip angle is transformed to the rear axle, and equation (2.23) can be modified to

$$\dot{\beta}_r = \dot{\psi} - \frac{l}{l_f m v_x} S_r \tag{2.25}$$

The dynamics of the tyre side forces are given by

$$\dot{S}_f = a \cdot \left(\overline{S}_f(\alpha_f) - S_f\right) = \frac{v_x}{0.03 v_x + 0.5}\left(C_f \alpha_f - S_f\right) \tag{2.26a}$$

$$\dot{S}_r = a \cdot \left(\overline{S}_r(\alpha_r) - S_r\right) = \frac{v_x}{0.03 v_x + 0.5}\left(C_r \alpha_r - S_r\right) \tag{2.26b}$$

where a is the initialisation transient and $C \cdot \alpha$ is the linearised tyre characteristics. The initialisation transient is the time range, given a certain speed, needed for the frictional force to saturate. The tyre stiffness has to be translated to the one-track model. C_f is calculated by applying the caster equation (2.6) on the cornering stiffness, to get the modified tyre stiffness C^*_{sf}, which is then multiplied by 2 to get the corresponding value for the one track model, i.e. $C_f = 2 \cdot C^*_{sf}$. For the rear axle, a multiplication by 2 is enough, since there is no caster, i.e. $C_r = 2 \cdot C_{sr}$.

The actuator dynamics can be modelled with a second order differential equation.

$$\ddot{\delta}_f = \frac{1}{T_f^2}\left(u_1 - D_f T_f \dot{\delta}_f - \delta_f\right) \tag{2.27a}$$

$$\ddot{\delta}_r = \frac{1}{T_r^2}\left(u_2 - D_r T_r \dot{\delta}_r - \delta_r\right) \tag{2.27b}$$

T is the time constant and D the damping ratio. The actuators will be added externally, and will not be included in the state space representation.

And finally, by adding up everything, a fourth order state space representation is obtained

$$\dot{x} = Ax + Bu \tag{2.28}$$

$$y = Cx + Du \tag{2.29}$$

with

$$A = \begin{pmatrix} 0 & 0 & \frac{l_f}{I_{zz}} & -\frac{l_r}{I_{zz}} \\ 1 & 0 & 0 & -\frac{l}{l_f m v_x} \\ a \cdot \left(-C_f \cdot \frac{l_f + \frac{I_{zz}}{l_f m}}{v_x} \right) & a \cdot C_f & -a & 0 \\ a \cdot \left(C_r \cdot \frac{l_r - \frac{I_{zz}}{l_f m}}{v_x} \right) & a \cdot C_r & 0 & -a \end{pmatrix} \tag{2.30}$$

$$B = \begin{pmatrix} 0 & 0 \\ 0 & 0 \\ a \cdot C_f & 0 \\ 0 & a \cdot C_r \end{pmatrix} \quad C = \begin{pmatrix} 1 & 0 & 0 & 0 \\ 0 & 1 & 0 & 0 \end{pmatrix} \quad D = \begin{pmatrix} 0 & 0 \\ 0 & 0 \end{pmatrix} \tag{2.31}$$

The transfer function of the state space model is

$$G(s) = D + C\left(sI - A\right)^{-1} B = \begin{pmatrix} g_{11}(s) & g_{12}(s) \\ g_{21}(s) & g_{22}(s) \end{pmatrix} \tag{2.32}$$

2.3 Model Parameters

The experimental vehicle used is an S-class, and is called *Techno Shuttle w220*. It has front and rear wheel electro-hydraulic steering, active suspension and 4 electrohydraulic brakes. The parameters and constraints needed for the design and in the simulation are given by table 2.2.

With the parameters from table 2.2, and a speed of $v_x = 14$ m/s, the transfer function of the model is

$$G = \begin{pmatrix} \frac{358.9744(s^2+7.692s+293)}{(s^2+9.354s+216.8)(s^2+6.03s+296.6)} & \frac{-512.8205(s^2+7.692s+205.1)}{(s^2+9.354s+216.8)(s^2+6.03s+296.6)} \\ \frac{358.9744(s+3.506)}{(s^2+9.354s+216.8)(s^2+6.03s+296.6)} & \frac{-293.0403(s^2+9.442s+223.7)}{(s^2+9.354s+216.8)(s^2+6.03s+296.6)} \end{pmatrix} \tag{2.33}$$

Table 2.2: Parameters and constraints of the car model

Parameter	**Unit**	**Remarks**	**w220**
C_f	$[N/rad]$	Front tyre stiffness	144000
C_r	$[N/rad]$	Rear tyre stiffness	283000
C_L	$[N/rad]$	Elasticity constant	10000
n_S	$[m]$	Lateral front wheel caster	0.055
δ_f	$[rad]$	Front wheel steering angle	$[-40°, 40°]$
δ_r	$[rad]$	Rear wheel steering angle	$[-5°, 5°]$
$\dot{\delta}_f$	$[rad/s]$	Front wheel steering angular velocity	$[-800°/s, 800°/s]$
$\dot{\delta}_r$	$[rad/s]$	Rear wheel steering angular velocity	$[-88°/s, 88°/s]$
I_{zz}	$[kg \cdot m^2]$	Mass moment of inertia	5000
m	$[kg]$	Vehicle mass	2364
l_f	$[m]$	Distance between the center of mass and the front axis	1.673
l_r	$[m]$	Distance between the center of mass and the rear axis	1.412
L	$[m]$	Distance between the front and the rear axis	3.085

3 Control Strategies and Specifications

3.1 Specifications

When discussing the specifications, there are four main concepts that have to be mentioned

- *Model matching.* From the modelled vehicle dynamics, mentioned in the introduction, the achievement of some particular driving dynamics is desired. The reference signals are the only interface to the unknown model and a good tracking of these references is desired. With this as a starting point, the objective is to make the plant behave just like the model, and in that way obtain the desired driving dynamics. To achieve this, a plant inverse can be calculated to generate the steering angles corresponding to the particular reference values. In the ideal situation, i.e. if the plant transfer function is perfectly known, the problem would be solved; the output would always be equal to the reference. But calculating the inverse is not a trivial matter, not only because of plant uncertainties. If the plant transfer function has unstable zero dynamics and time delays, giving it non-minimum phase characteristics, the inverse would become unstable. This shows the difficulties of obtaining a good inverse. However, an approximate inverse provides a steering angle reference trajectory, and feedback can be used to stabilise around this nominal trajectory.

- *Robustness to system uncertainties.* To handle uncertainties of the real plant, a feedback has to be used to handle small excitations of the actual trajectory from the reference trajectory given by the inverse above.

- *Disturbance rejection.* Uneven road surface, wind disturbances and inclination of the road are examples of disturbances that can appear and that have to be taken care of by the feedback.

- *System integrity.* The system has to be stable in all situations. This means that even if one actuator fails, the remaining active controller should be able to keep the system in stability. In this particular case, the specification is restricted to comprise only rear actuator failure. With a front actuator failure, and the hard constraints on the rear wheel steering angle, a stabilisation would be very hard to achieve. Other factors that might put system integrity to the test, and brake the feedback loop, could be sensor failure or hitting steering angle constraints.

The closed loop system should have low pass characteristics. It must have a specified closed loop bandwidth (or open loop crossover frequency, which is almost equivalent), and large enough phase and gain margin to guarantee stability. A high roll-off is needed to achieve good noise reduction, to protect the actuators and to handle high frequency uncertainties. Furthermore, the design has to be resistant to a certain time delay. This will, depending on the magnitude of the time delay, introduce a reduction in the phase margin of the open loop system. Thus, the damping will decrease, and perhaps the stability will be put at risk as well. Because of this, it is of huge importance to design the controllers such that the system has enough phase margin and in that way guarantee the system stability. The open loop specifications are given in table 3.1.

Table 3.1: Specifications

bandwidth	3 Hz = 18.8 rad/s
damping	0.5
time delay	20 ms = 0.020 s
settling time	max. 0.5 s

The specified time delay will give a reduction in phase margin ($\Delta\phi$) by $0.020 \text{ s} \cdot 18.8 \text{ rad/s} = 0.376 \text{ rad} = 21$ degrees at the crossover frequency. A damping (D) of 0.5 is equivalent to a phase margin of 51 degrees, according to table 3.2 [Burmeister]. By taking the time delay into account, the specification of the phase margin has to be changed from the original 51 degrees to 72 degrees.

Table 3.2: Connection between damping and phase shift

D	0.1	0.2	0.3	0.4	0.5	0.6	0.7	0.8	0.9
$\Delta\phi$	11.4°	22.6°	33.3°	43.1°	51.8°	59.2°	65.2°	69.9°	73.5°

3.2 The Feedforward

Although feedforward is the topic of this section, a more general description has to be made, involving both feedforward and feedback. Some ideas will be given on how feedforward can be combined with feedback. The feedback, however, will be described more in detail in section 3.3 and in chapter 4.

Attaining a desired system response as specified by a system transfer function $T(s)$, and simultaneously achieving sufficient feedback to handle

uncertainties and disturbances acting on the plant, requires a configuration with at least two degrees of freedom. The general design paradigm employed here will be the so called two degree of freedom design. With a reference trajectory generator, for example the human driver, as the starting point, the objective is to obtain a good trajectory following. From the reference trajectory, a nominal state space and plant input trajectory is generated using a full nonlinear plant description. This reference tracking is the first degree of freedom. The second degree of freedom uses linear theory to deal with disturbance rejection, stabilisation and robustness to system uncertainties. In this way the problem is divided into one feedforward tracking and one feedback stabilisation part. Experiments and simulations have shown that stabilisation around a nominal trajectory allows a more aggressive response for nonlinear systems [Nieuwstadt]. The system can be divided in two parts, one linear and one nonlinear. Eventually they will be combined to obtain the paradigm described above.

3.2.1 Linear system

Several different structures can be used to describe the two degree of freedom configuration. The structure used here is shown in fig 3.1. The significant feature of any such structure is that the system transfer function T and the system sensitivity function S can be independently realised. They fix the values of K_2 and K_1. With

$$T_1(s) = (I + G(s)K_1(s)))^{-1} G(s)K_1(s) \tag{3.1}$$

as the closed loop transfer function of the feedback loop and K_2 as the feedforward precompensation, the system equation can be written as

$$T_1(s) \cdot K_2(s) = T(s) = \begin{pmatrix} t_{11}(s) & t_{12}(s) \\ t_{21}(s) & t_{22}(s) \end{pmatrix} \tag{3.2}$$

and the sensitivity function

$$S(s) = (1 + G(s)K_1(s))^{-1} \tag{3.3}$$

The feedforward pre-compensation is used to compensate for the dynamics in the feedback loop. Even though a coupling design is used for the feedback (as will be seen in chapter 4), a significant degree of decoupling is desired for the system transfer function T. If, for example, a yaw rate and a side slip angle reference is used, it would make sense if the outputs do not contain any significant cross-coupling with the references; The yaw rate output should not depend on the side slip angle reference, and vice versa. The

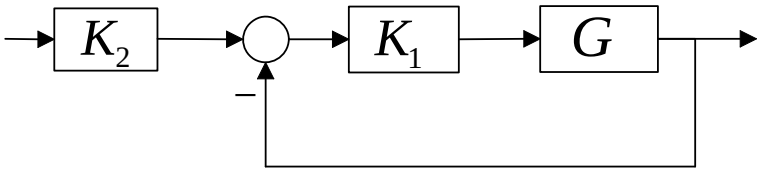

Figure 3.1: The two-degree-of-freedom structure.

feedforward compensator can be designed in such a way, that a decoupling is obtained. A K_2 that decouples the system would look as follows:

$$K_2(s) = T_1(s)^{-1} \cdot \begin{pmatrix} t_{11}(s) & 0 \\ 0 & t_{22}(s) \end{pmatrix} \tag{3.4}$$

However, a pre-compensator like this might be difficult to implement. If it contains pure derivatives, it would have to be approximated, and the real values of K_1 and G might differ from the values used in the calculations. In the steady state, a pre-compensator is easily obtained. The system steady state equation would be

$$T = T_1(0) \cdot K_2(0) = \begin{pmatrix} 1 & 0 \\ 0 & 1 \end{pmatrix} \tag{3.5}$$

and a steady state pre-compensator can be calculated. It would give a correct tracking, at least for low frequencies.

3.2.2 Nonlinear system

For a nonlinear system, a controller is used to stabilise around a nominal trajectory. The trajectory is generated from some realisable inverse of the vehicle model using model matching, and is independent of the controller. It generates a feedforward control signal used as input to the plant. Furthermore, it has to provide information about the states, which is needed in the feedback. Figure 3.2 illustrates the feedforward.

The most likely approach would be a steady state feedforward inverse. By calculating the dc-gain of the system matrix, $|G_{vehicle}(0)|$, and inverting it, an inverse will be obtained that is at least a good approximation in the steady state. This is a sufficient solution only if the gain of the plant is more or less constant in the range of the specified bandwidth.

A more general inverse would require minimum phase properties of the plant transfer function. This would make an inverse hard to realise. Instead, a common way of doing it is using a feedback loop and a high gain controller, according to figure 3.3.

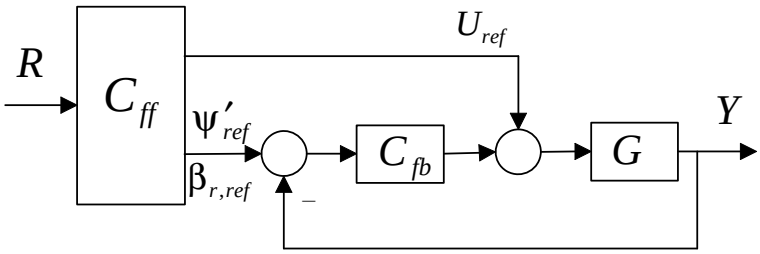

Figure 3.2: Control using feedforward and feedback.

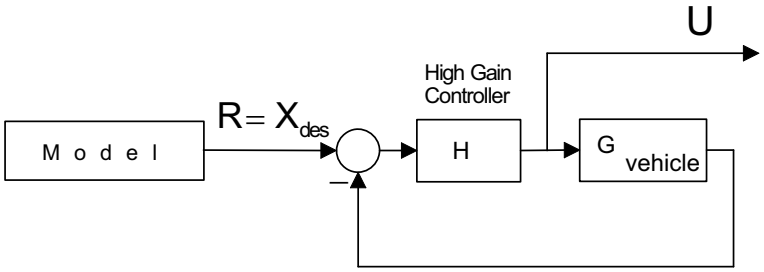

Figure 3.3: Feedback loop with high gain controller used to generate the system inverse, giving U_{ref}.

3.2.3 Combining the nonlinear feedforward and the linear feedback

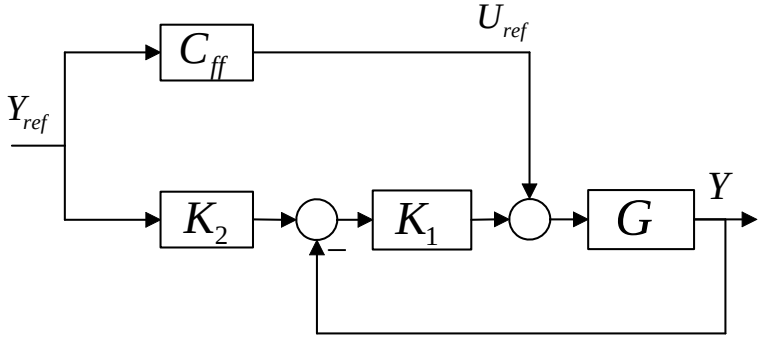

Figure 3.4: Two-degree-of-freedom design combining the nonlinear and the linear system.

A combination of the linear and the nonlinear approach can be done according to figure 3.4 and the problem will be investigated in a linear setting. The feedback loop is used for stabilisation around the nominal trajectory and the input-output relationship that describes the tracking performance would look according to equation (3.6).

$$Y = T \cdot Y_{ref} = (I + GK_1)^{-1} (GK_1K_2 + GC_{ff}) Y_{ref} \tag{3.6}$$

With some kind of inverse, $C_{ff} = \hat{G}^{-1}$, as the starting point, the transfer function would be

$$T = (I + GK_1)^{-1} \left(GK_1K_2 + G\hat{G}^{-1} \right) = (I + GK_1)^{-1} (GK_1K_2 + G_1) \tag{3.7}$$

where $G_1 = G\hat{G}^{-1}$ has low pass characteristics and is some kind of "approximate" unit matrix. The second factor is the sensitivity function with low gain for low frequencies. This would give a transfer function for low frequencies according to

$$T_{lowfreq} = (I + GK_1)^{-1} GK_1K_2 \tag{3.8}$$

and allowing a shaping of the feedforward K_2 to obtain the desired closed loop characteristics for low frequencies. If the whole frequency spectrum is considered, and the feedforward is set to $K_2 = G_1$, the transfer function from reference to output would be

$$Y = (I + GK_1)^{-1} (GK_1G_1 + G_1) Y_{ref} = G_1 \cdot Y_{ref} \tag{3.9}$$

This would result in a considerable amount of decoupling (recall that G_1 is close to an unit matrix), and give the system low pass characteristics.

3.3 The Feedback

There are different theories and approaches regarding control of the yaw rate and side slip angle of a car. Here are some of them:

- *Decoupling by inverting the system equation and using PD-control (ENT-controller).* The integral part in the controller is replaced by a disturbance observer.
- *Decoupling with constraints on the side slip angle.* Switching between ENT- and SM2-controller.
- *Independent control of front and rear axle (SM2/BSR).* Yaw rate control with the front axle and side slip angle control with the rear axle.

- *Decoupling through coordinate transformation.* Generalisation of the first approach.
- *Control without using the side slip angle (OBETA).*
- *Coupling by Individual Channel Design.* The design used in this work. Made in the frequency domain, and not in the time domain as the previous ones. Described in chapter 4.

In previous work, decoupled controllers are used, where system integrity cannot be guaranteed. Furthermore, the difficulties of accommodating time delays and unstructured uncertainties when doing state space design are extensive and have to be mentioned.

The feedback design will be based on the bicycle model from chapter 2.2. Nothing says that this model is a close representation of a real car, mainly because of the nonlinear tyre forces that appear when driving a real car, and which are not considered in the model. But in the linear region and for small signals the bicycle one track model should be sufficient. The nonlinear differential system equation is $\dot{x} = f(x, u)$ and a linearisation can be done in two ways:

1. Around an equilibrium point, x_0, u_0, that satisfies $f(x_0, u_0) = 0$, or
2. Around a nominal reference trajectory, x_{ref}, u_{ref}, that satisfies

$$f(x_{ref}, u_{ref}) = \dot{x}_{ref} \tag{3.10}$$

In this particular case, this is a more suitable approach.

Some deviations in the behaviour of the model compared to a real car can be accepted, on condition that the feedback is designed in such a way that these uncertainties are suppressed.

There also exist constraints on the steering angles, giving nonlinear actuator dynamics. The front actuator is limited to 40 degrees and the rear to 5 degrees. If one of them saturates, and an integrator is used in the controller, the resulting windup will cause large overshoots or even make the system unstable. This is something that has to be taken into consideration when making the design, by constructing an appropriate anti-windup. It is done according to [Åström], and will not be presented here.

Further, the lightly damped closed loop channel poles change with speed. This implies that the feedback design has to be done for different speeds such that the specifications are fulfilled for different driving situations.

4 Coupled Feedback Design with Diagonal Controller - Individual Channel Design

To guarantee the global stability of a car with front wheel steering, or, in other words, preventing it from losing traction, the side slip angle must be kept under control and under a certain threshold. If it exceeds the critical value, the yaw rate control has to be switched to a pure side slip angle control. Simultaneous control of both quantities is impossible with only front wheel steering. If, instead, a vehicle with both front and rear wheel steering is used, control of both quantities, i.e. the side slip angle and the yaw rate, is enabled.

Individual Channel Design (ICD) will be used for the two-variable feedback design in the frequency domain. It is an application-oriented design, and it starts from the premise that feedback design is interactive; it involves an interplay between specifications, uncertain plant characteristics, and the multivariable feedback design process itself. Each of these will be present in this work, at one point or another.

4.1 Theory

The control approach that is used today is based on decoupled yaw rate and side slip angle controllers, or compensators. This means that one compensator, with front wheel steering angle as control signal, is used for controlling the yaw rate, and another one, with rear wheel steering angle as control signal, controls the side slip angle. The two compensators are designed, in the time domain, independently of one another, and the mutual interaction is not considered. Figure 4.1 shows the entire system and it can be seen that the yaw rate not only depends on the yaw reference input but also on the side slip angle and vice versa.

This allows us to define a transfer matrix of the plant

$$G(s) = \begin{pmatrix} g_{11}(s) & g_{12}(s) \\ g_{21}(s) & g_{22}(s) \end{pmatrix} \tag{4.1}$$

according to equation (2.32), with the reference input and resulting output

$$R = \begin{pmatrix} r_1 \\ r_2 \end{pmatrix} = \begin{pmatrix} \dot{\psi}_{ref} \\ \beta_{r,ref} \end{pmatrix} \qquad Y = \begin{pmatrix} y_1 \\ y_2 \end{pmatrix} = \begin{pmatrix} \dot{\psi} \\ \beta_r \end{pmatrix} \tag{4.2}$$

And the multivariable controller, consisting of two single compensators k_i (i=1,2), can be described by a diagonal matrix

$$K(s) = \begin{pmatrix} k_1(s) & 0 \\ 0 & k_2(s) \end{pmatrix} \tag{4.3}$$

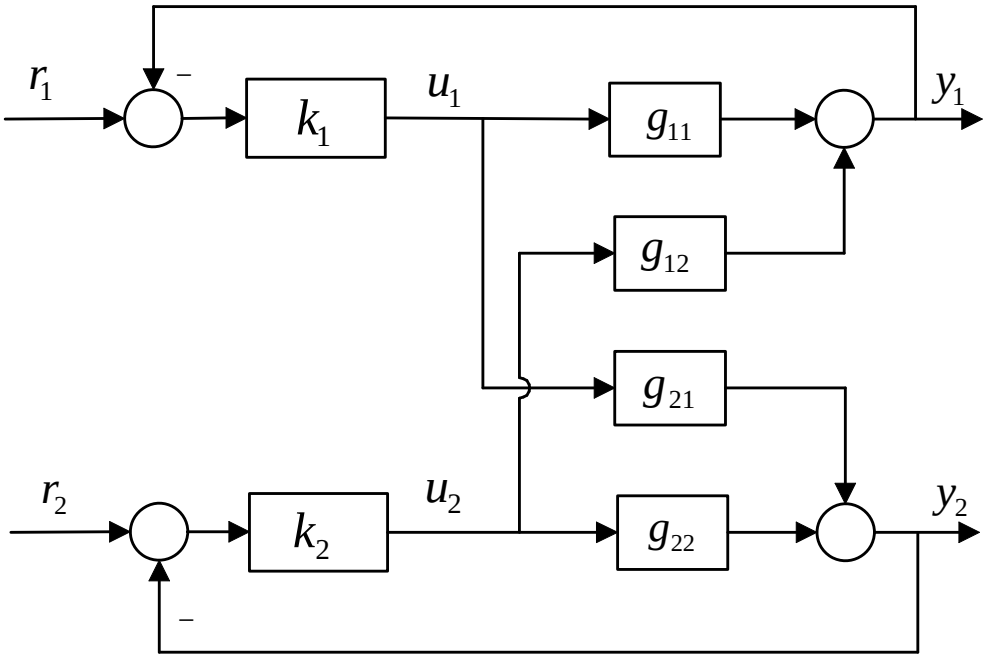

Figure 4.1: The Complete System

This results in a multivariable feedback loop where an input u_i and a reference r_i can be assigned to each output y_i (i=1,2) from the process. Each compensator k_i uses the output information y_i and the reference value r_i to give the control signal u_i. Under these assumptions one can, without any loss of information, split this double-input double-output control loop into two single-input single-output (SISO) loops, each consisting of a channel, C_i.

For a multivariable system we have, in matrix form, the expression for the feedback loop

$$Y = (I - GK)^{-1} GKR = T_1 R = \begin{pmatrix} \frac{C_1(s)}{1+C_1(s)} & \frac{g_{12}(s)}{g_{22}(s)} \frac{h_2(s)}{1+C_1(s)} \\ \frac{g_{21}(s)}{g_{11}(s)} \frac{h_1(s)}{1+C_2(s)} & \frac{C_2(s)}{1+C_2(s)} \end{pmatrix} R \quad (4.4)$$

where

$$C_i(s) = k_i(s) g_{ii}(s) \left(1 - \gamma(s) h_j(s)\right) \quad (4.5)$$

is the open loop SISO transfer function of the channel,

$$\gamma(s) = \frac{g_{12}(s) g_{21}(s)}{g_{11}(s) g_{22}(s)} \quad (4.6)$$

is the complex-frequency multivariable structure function and describes the

internal coupling of the plant, and

$$h_j(s) = \frac{k_j(s)g_{jj}(s)}{1 + k_j(s)g_{jj}(s)} \tag{4.7}$$

describes the impact of the compensator k_j on the i:th $(i \neq j)$ control loop. The result above gives us the structure according to fig 4.2. In this way the

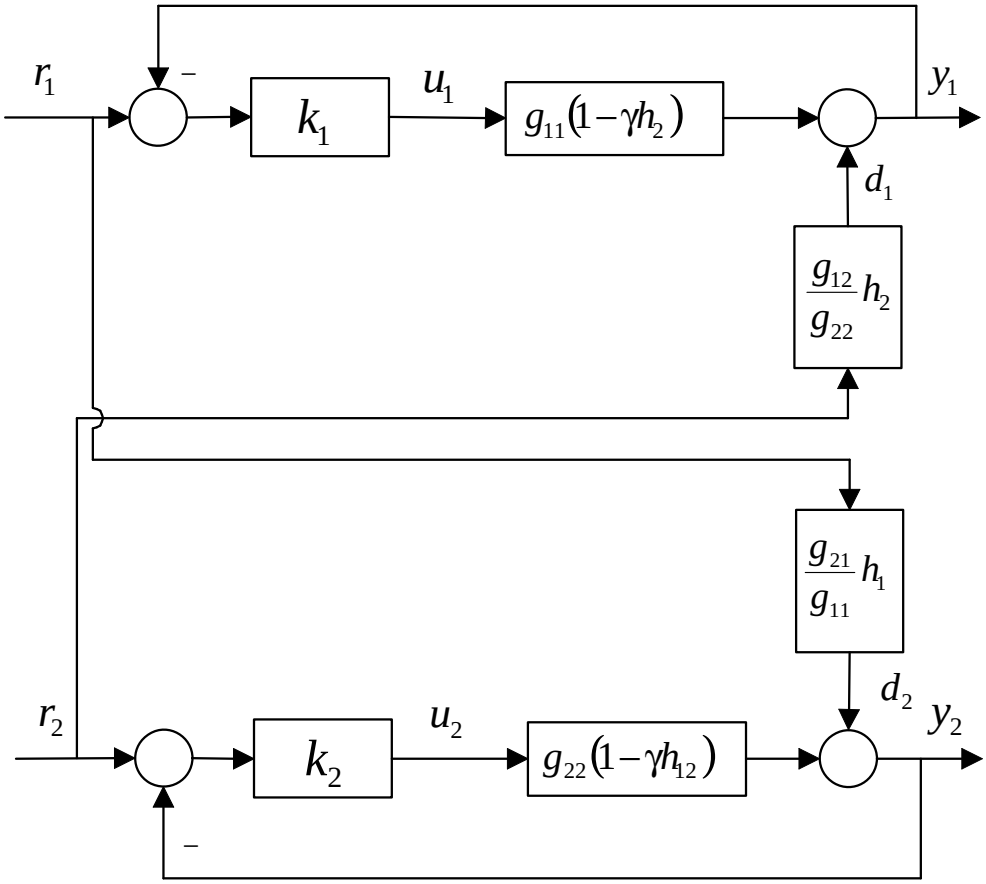

Figure 4.2: The Two Channels

multivariable control problem decomposes into two single variable channels, each enclosed within a feedback loop with a compensator that must be designed to meet the unique channel specifications. Each channel C_i is subject to the disturbance d_i $(i = 1, 2)$ and the behaviour will be affected not only by the compensator of the channel itself, but also on the behaviour of the other channel C_j $(j \neq i)$; when the magnitude of the structure function $\gamma(s)$ is much less than one the loop signal interaction is low, otherwise, loop signal interaction is high.

The pole-zero structure of the two channels, assuming that no pole-zero cancellations occur within $\gamma(s)$, is shown in table 4.1. In equation (4.6) it can be observed that the poles of g_{12} and g_{21} and the zeros of g_{11} and g_{22} are the poles of $\gamma(s)$. However, the zeros of h_2 in equation (4.7) include the zeros of g_{22} but not g_{11}, which in that case are poles of $(1-\gamma h_2)$, and will cancel out the zeros of g_{11} in front of the bracket. Hence, the zeros of $g_{11}(1-\gamma h_2)$ are the zeros of $(1-\gamma h_2)$ and the poles of $g_{11}(1-\gamma h_2)$ are the poles of g_{11}, g_{12}, g_{21} and h_2. The pole zero structure of C_2 is similar.

Table 4.1: Open-loop channel poles and zeros

	Zeros	**Poles**
Channel C_1	Zeros of $(1-\gamma h_2)$	Poles of $g_{11}, g_{12}, g_{21}, h_2$
Channel C_2	Zeros of $(1-\gamma h_1)$	Poles of $g_{22}, g_{12}, g_{21}, h_1$

Individual Channel Design on the original double-input double-output cross-coupled multivariable system is valid irrespective of the degree of cross-coupling. This extension is shown in [Leithead, O'Reilly].

4.2 Adding Actuators

Second order actuators from equations (2.27a) and (2.27b) are used, with the transfer functions

$$H_{front} = \frac{1}{1 + D_f T_f s + T_f^2 s^2} \tag{4.8}$$

$$H_{rear} = \frac{1}{1 + D_r T_f s + T_f^2 s^2} \tag{4.9}$$

and time constant and damping according to table 4.2. The transfer function of the front actuator (equation (4.8)) is multiplied by $g_{11}(s)$ and $g_{21}(s)$ and, similarly, the transfer function of the rear actuator (equation (4.9)) is multiplied by $g_{22}(s)$ and $g_{12}(s)$. See figure 4.3.

The entire system would be

$$G_{PT2} = \begin{pmatrix} H_{front} g_{11} & H_{rear} g_{12} \\ H_{front} g_{21} & H_{rear} g_{22} \end{pmatrix} \tag{4.10}$$

Table 4.2: Actuator parameters.

	Time constant T (s)	**Damping** D (s)
Front actuator	0.012	0.612
Rear actuator	0.0072	0.612

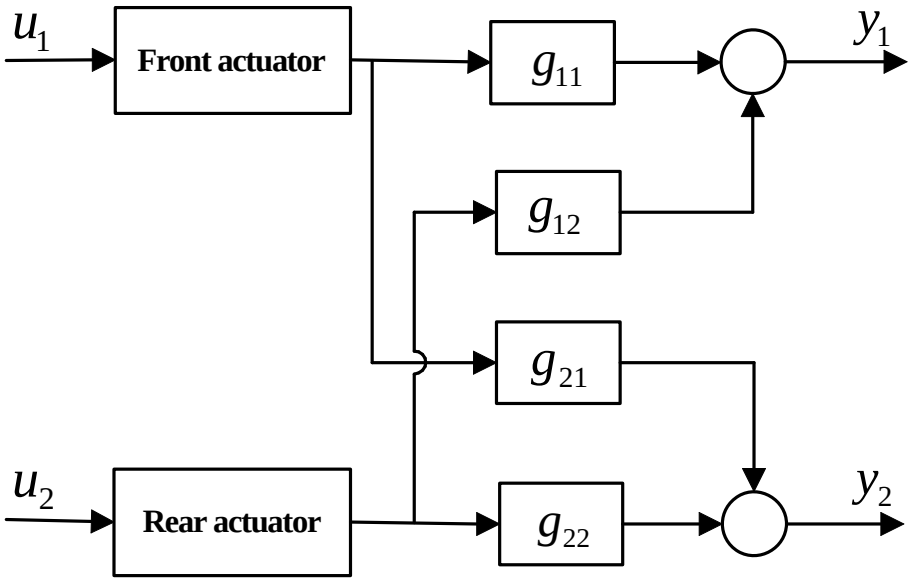

Figure 4.3: The connection between the plant and the actuators

4.3 The Main Advantages and Disadvantages

As mentioned in the introduction, the control system has to be robust to plant uncertainties, and a failure of one actuator must not destabilise the system. The actuators are connected to the plant according to figure 4.3. It should be recalled that the open loop transmittance C_1 is the transmittance between r_1 and y_1, with the feedback loop from plant output 1 to control input 1 open, but with the other feedback loop closed. And likewise for channel 2. Hence, a failure of one actuator means that the feedback loop of the channel C_i, which the actuator concerned belongs to, is broken. The subsystem transfer function in question, h_i, can be set equal to zero. The

other channel will, consequently, have a rather simple structure:

$$C_j(s) = k_j(s)g_{jj}(s) \quad (i \neq j) \tag{4.11}$$

and it is of great importance to make sure that the remaining active compensator, k_j, can stabilise the system. The performance, and in particular the stability, of the closed loop system under a failure of one of the feedback loops may thus be determined directly from inspection of the poles of the corresponding open loop channel transmittance. In other words, *system integrity* after feedback loop failure is guaranteed provided the following two conditions are satisfied:

1. all the individual plant transfer functions $g_{ij}(s)$ $(i, j = 1, 2)$, are stable;
2. the subsystem transfer functions $h_i(s)$ $(i = 1, 2)$, are stable.

With the decoupled system, this would not be self-evident.

When designing the controller for a plant, one of the primary requirements is robustness; that is, to ensure that the resulting closed loop performance is not badly degraded by plant uncertainty. This is done by designing controllers such that sufficiently large phase and gain margins are obtained to guarantee satisfactory closed loop performance even in the presence of plant uncertainties. But, this is only valid in the SISO case. For a double-input double-output system, enough phase and gain margins are not sufficient for robustness to plant uncertainties. There are two reasons for that: excessive phase/structural sensitivity to plant parameter uncertainty at frequencies at/below the channel crossover frequency. This leads to the following additional requirement [Leithead,O'Reilly]:

- For robustness of the closed loop system stability to general plant parameter uncertainty, it is necessary that the Nyquist plots of the multivariable structure functions $\gamma h_i(s)$ $(i = 1, 2)$ do not go close to the point (1,0) at frequencies near or less than the channel crossover frequencies.

In the requirement above, large plant uncertainty is implicitly assumed. When the plant is well known, single-loop control can be used with the decoupled system.

The feedback design is carried out in the frequency domain. The conversion from state space representation to transfer function means that information about the internal structure of the plant is lost. Furthermore, the design is restricted to the linear region.

4.4 The Design Procedure

Because of the mutual dependency between the channels, the design of this two individual channel system is done by iteration, one channel at a time, until the specifications are met for both channels.

For each design step, the root-locus plot and the bode diagram of the closed loop channel have to be studied and necessary modifications have to be made to the compensator. After that is done, the step response should behave satisfactory, with enough damping, short rise time and settling time.

The design paradigms used are as follows:

- *Poles to increase the roll-off at high frequencies.* These poles are usually introduced at frequencies of 4 times the crossover frequency or higher ($4 \cdot 18.8$ rad/s).
- *Complex zero pair to cancel out lightly damped complex poles.* The plant has one lightly damped complex pole pair. A complex zero pair has to be put such that a satisfactory cancellation occurs. It should be kept in mind that the position of the pole pair can never be perfectly known, and only an approximate cancellation can be obtained.
- *Integrator pole at the origin to eliminate the steady state error.*
- *Correct the control gain such that the specifications for the bandwidth are met.*
- *Scheduling of the controller gain and the complex zero pair with respect to speed.* The pole-zero position of the two channel transfer functions is speed dependant. This requires scheduling of the compensators, such that correct bandwidth and pole cancellation is obtained for all speeds.

5 Feedback Design - Results

The second order actuators have high frequency poles with low damping. Just cancelling the actuators poles by zeros would be unrealistic since the lightly damped poles move with changing actuator parameters. Instead, an approach with no actuator cancellation can be used (according to section 4.4):

$$k_1 = \frac{K_1 (s - z_1)(s - z_1^*)}{s(s + 80)} \tag{5.1}$$

$$k_2 = \frac{K_2 (s - z_2)(s - z_2^*)}{s(s + 80)} \tag{5.2}$$

The dominant pole structure of the plant looks according to figure 5.1. After a few iterations, by placing the compensator complex zero right on the

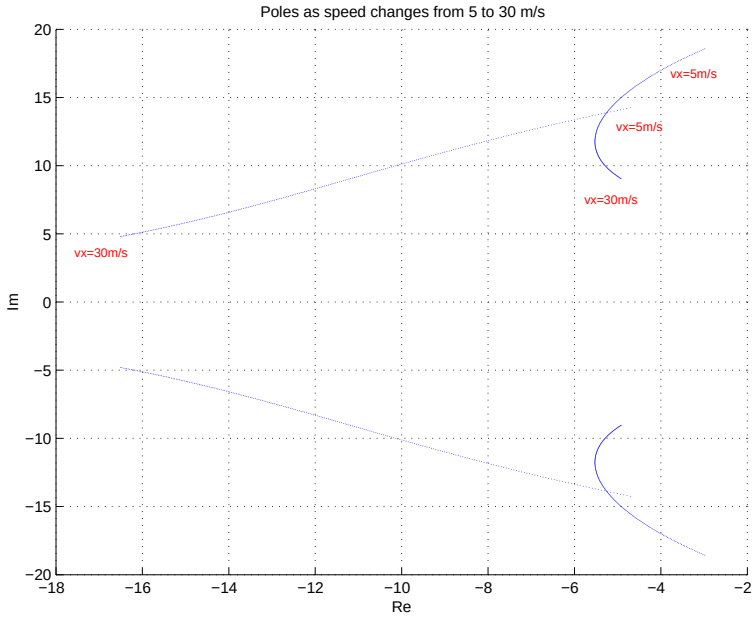

Figure 5.1: Poles of the plant as a function of speed

lightly damped complex pole of the plant and adjusting the gain to get the specified bandwidth, the zero-gain structure in table 5.1 and the root-locus plots and bode diagrams in figures 5.2 to 5.5, are obtained. The speed is $v_x = 14m/s$.

The phase margins and cross-over frequencies are shown in table 5.2.

In the bode plot of the first channel (figure 5.3), a plateau around the frequencies of the controller complex zero (15 rad/s) can be observed. The

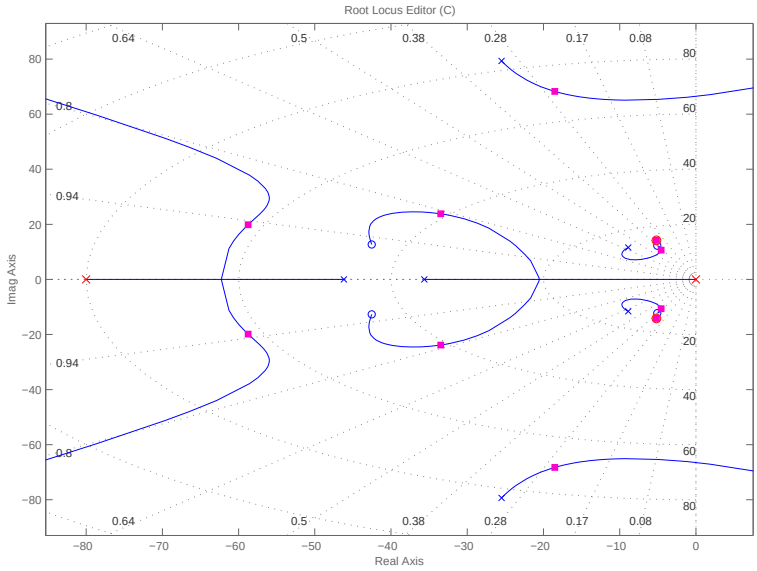

Figure 5.2: Channel 1 closed after 2 iterations. Compensators k_1 and k_2, $v_x = 14m/s$. Second order actuator.

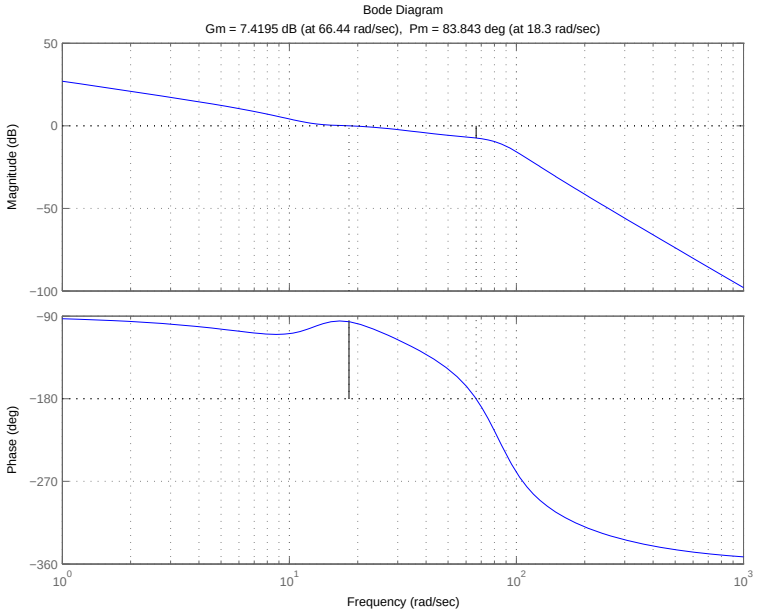

Figure 5.3: Bode plot of channel 1 with compensators k_1 and k_2 after 2 iterations.

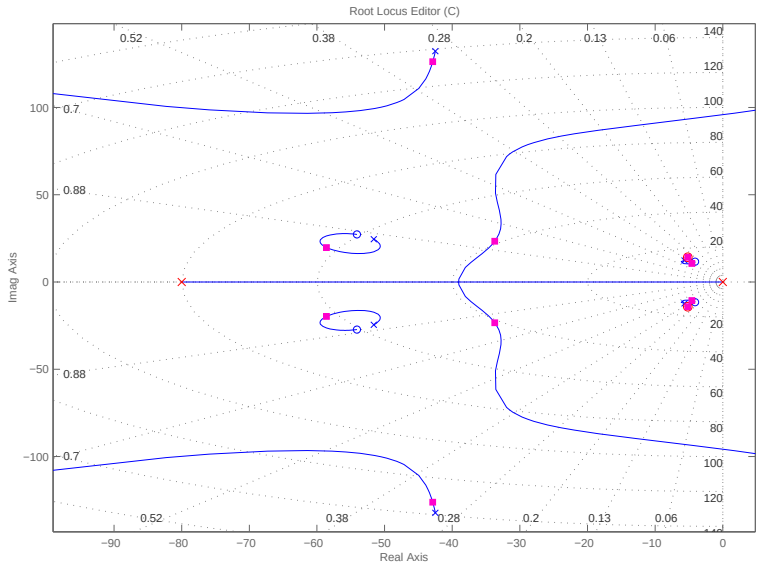

Figure 5.4: Channel 2 closed after 2 iterations. Compensators k_1 and k_2, $v_x = 14m/s$. Second order actuator.

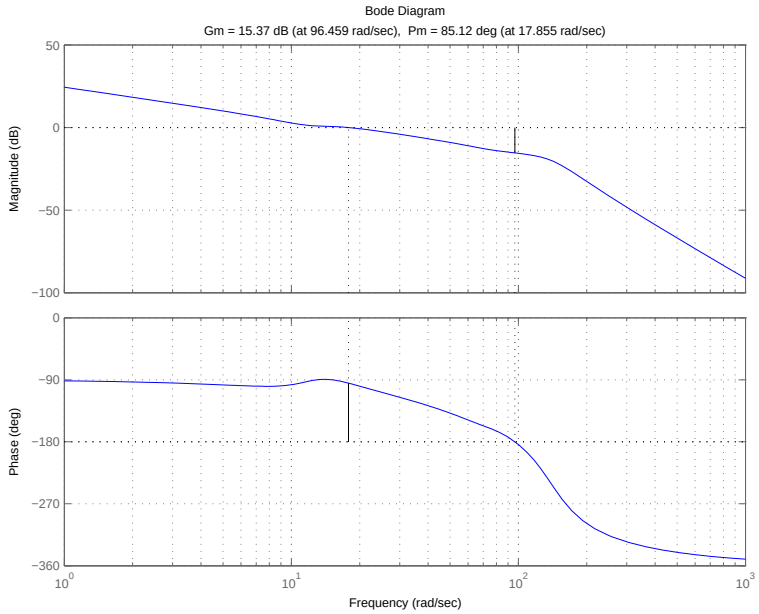

Figure 5.5: Bode plot of channel 2 with compensators k_1 and k_2 after 2 iterations.

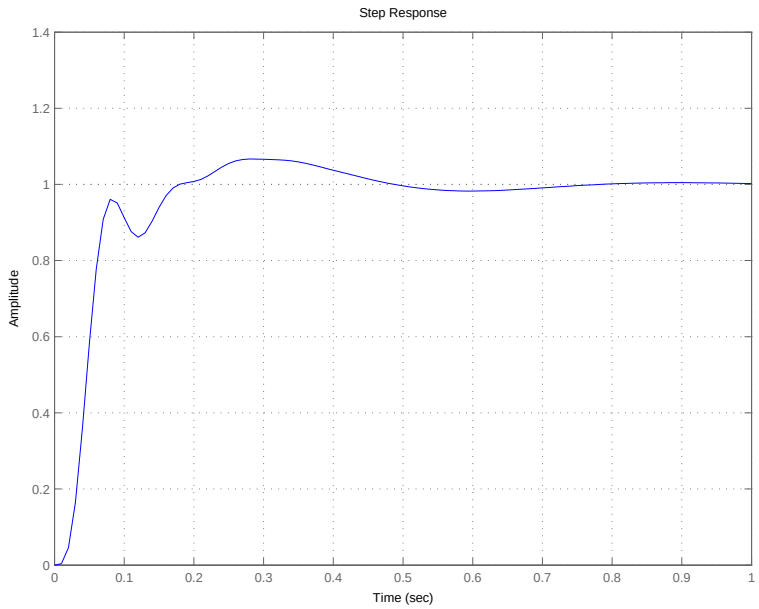

Figure 5.6: Step response of C_1, after 2 iterations. Compensators k_1 and k_2, $v_x = 14m/s$. Second order actuator.

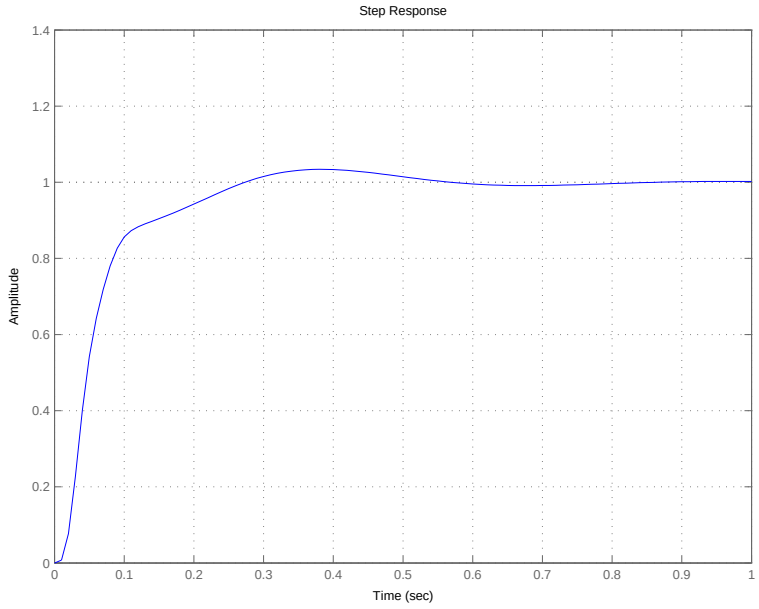

Figure 5.7: Step response of C_2, after 2 iterations. Compensators k_1 and k_2, $v_x = 14m/s$. Second order actuator.

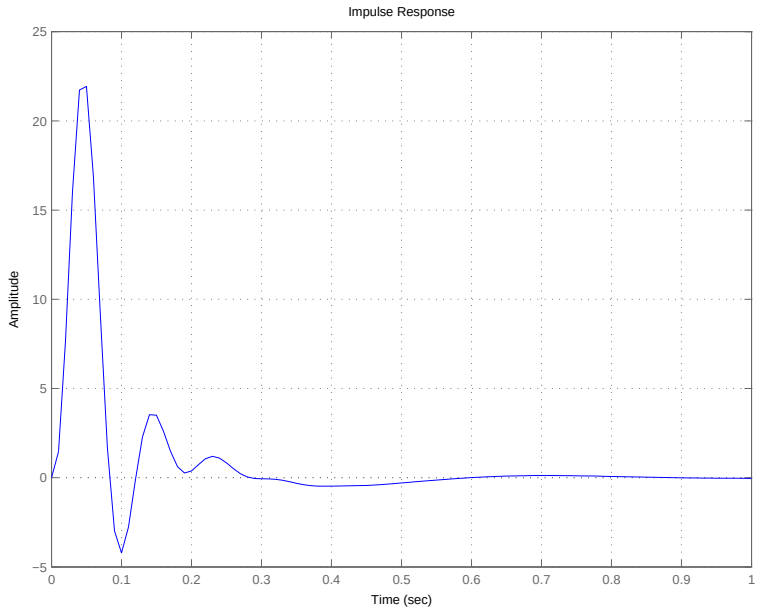

Figure 5.8: Impulse response of C_1, after 2 iterations. Compensators k_1 and k_2, $v_x = 14m/s$. Second order actuator.

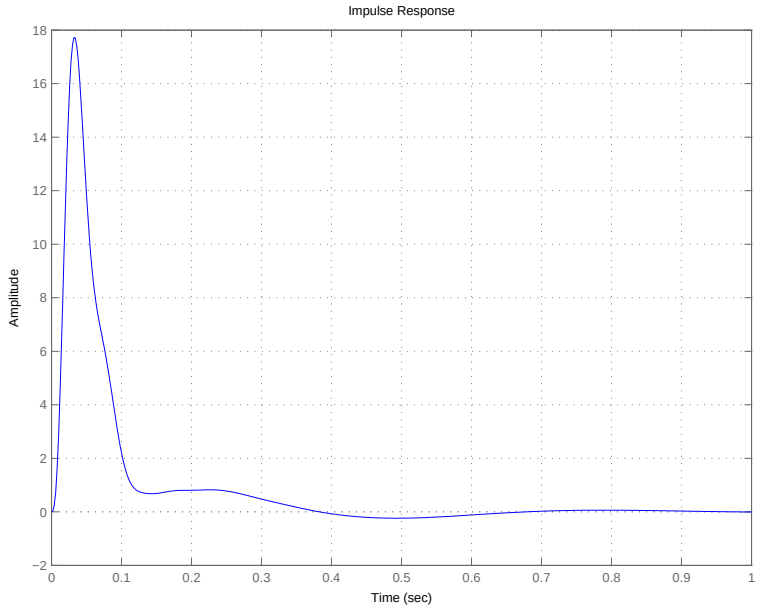

Figure 5.9: Impulse response of C_2, after 2 iterations. Compensators k_1 and k_2, $v_x = 14m/s$. Second order actuator.

Table 5.1: Gain, and complex zero pair, of the two compensators with second order actuator and $v_x = 14$.

	Gain K_i $(i = 1, 2)$	**Zero** z_i $(i = 1, 2)$
Channel C_1	2.4692	$-5.1780 + 14.1772i$
Channel C_2	-5.8253	$-5.1780 + 14.1772i$

Table 5.2: Phase margin and crossover frequency of both channels, with second order actuator and $v_x = 14$.

	Phase margin, $\Delta\phi$	**Cross-over frequency** (rad/s)
Channel C_1	84°	18.3
Channel C_2	85°	17.9

gain there is only 1.07 (0.6dB), which might aggravate the closed loop performance in terms of noise rejection around those frequencies. Furthermore, the slightest uncertainty in compensator gain might change the crossover frequency and phase margin significantly. The gain margin of the first channel is also very low. This gives, as can be seen in figure 5.6, lightly damped modes in the step response, caused by bad damping of the actuator poles. If the specifications are relaxed for the first channel, by allowing a lower bandwidth, this problem can be solved with a modified first compensator. There will be a loss in performance, but in this case a tradeoff has to be done between entirely meeting the specifications and having a high performance. The resulting zero-gain structure, root-locus plot and bode diagram of the two channels, after two iterations, are shown in table 5.3 and figures 5.10 to 5.13. The decreased performance of channel 1 compared to channel 2 can be seen in the step and impulse responses in figures 5.14 to 5.17. Table 5.4 shows the phase margins and crossover frequencies. The closed loop gain for frequencies within the bandwidth has to be close to 1 for both channels. This is illustrated in figures 5.18 and 5.19.

Many different solutions for design have been tried out, and the function-

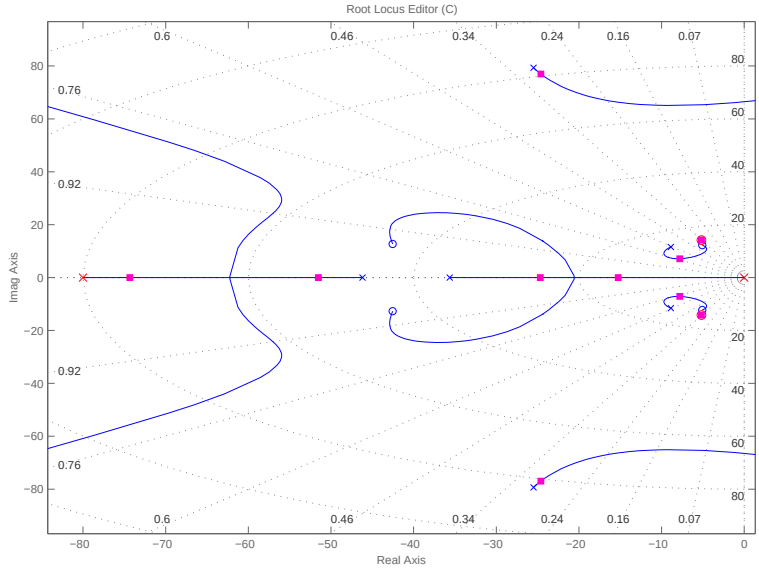

Figure 5.10: Channel 1 closed after 2 iterations. Modified compensators k_1 and k_2, $v_x = 14m/s$. Second order actuator.

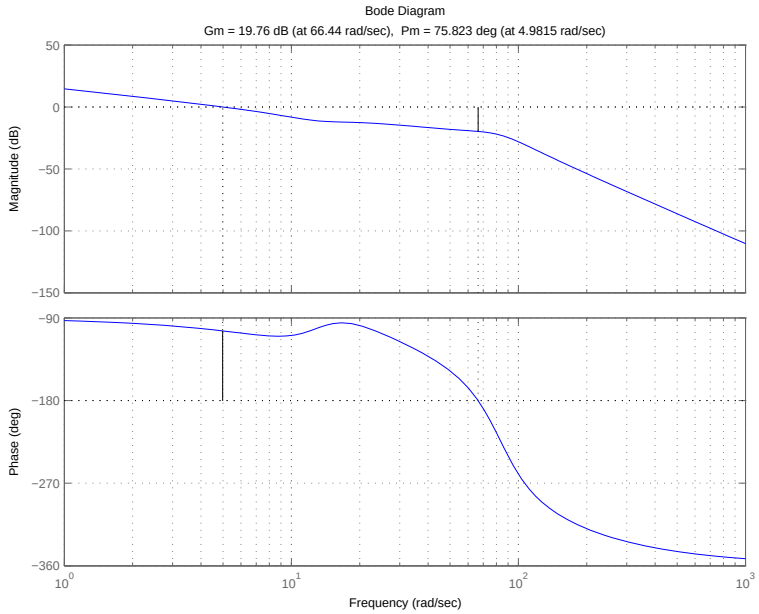

Figure 5.11: Bode plot of channel 1 with modified compensators k_1 and k_2 after 2 iterations. The crossover frequency is decreased to 5 rad/s.

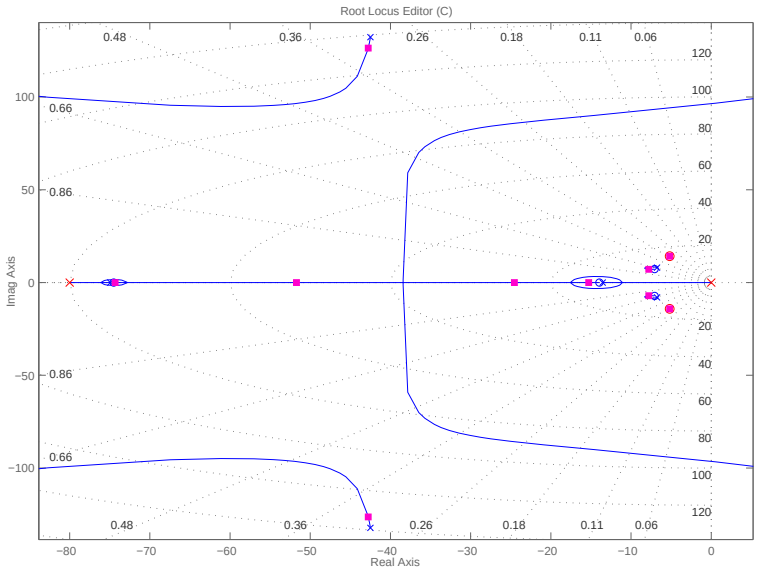

Figure 5.12: Channel 2 closed after 2 iterations. Modified compensators k_1 and k_2, $v_x = 14m/s$. Second order actuator.

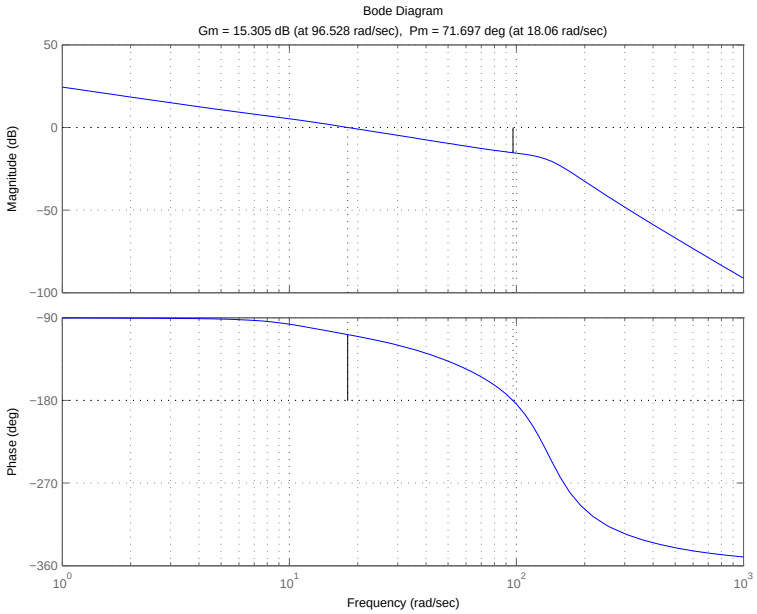

Figure 5.13: Bode plot of channel 2 with modified compensators k_1 and k_2 after 2 iterations.

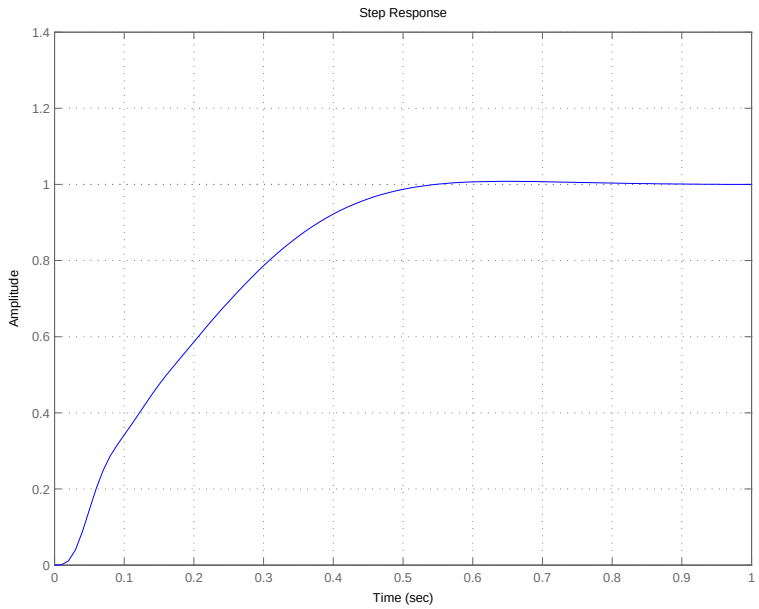

Figure 5.14: Step response of C_1, after 2 iterations. Modified compensators k_1 and k_2, $v_x = 14m/s$. Second order actuator.

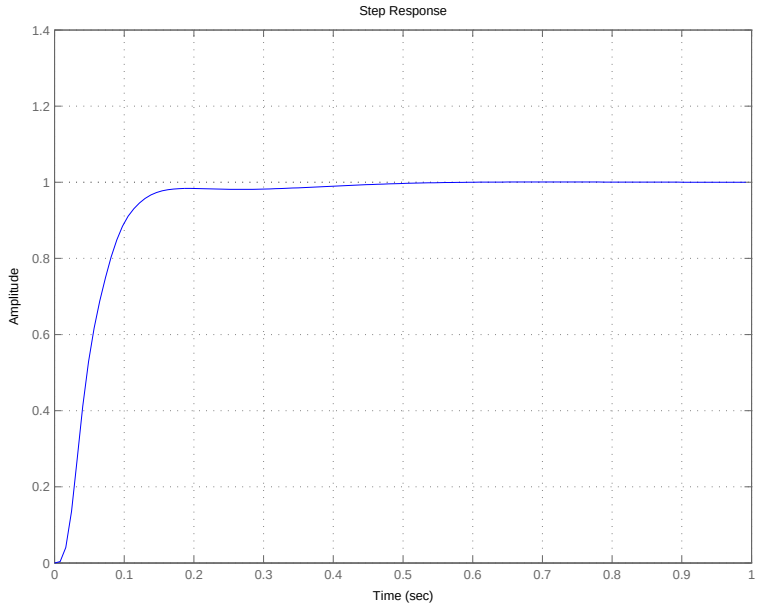

Figure 5.15: Step response of C_2, after 2 iterations. Modified compensators k_1 and k_2, $v_x = 14m/s$. Second order actuator.

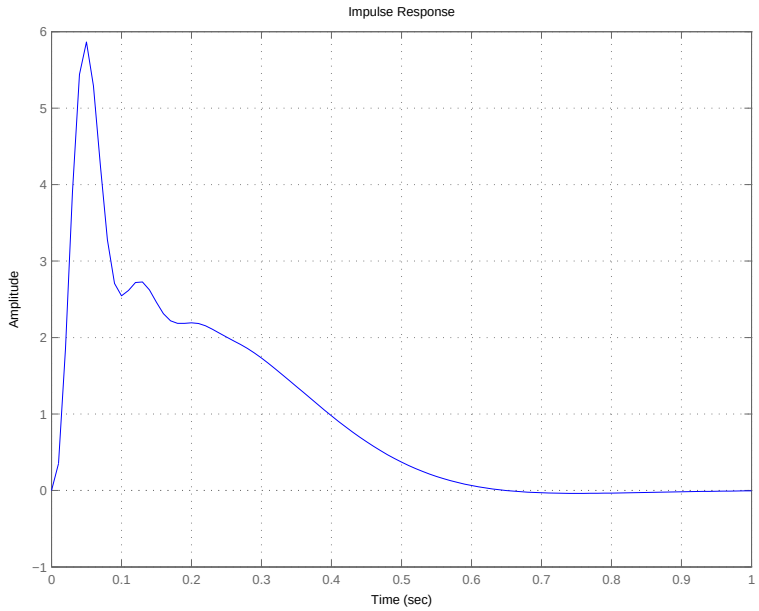

Figure 5.16: Impulse response of C_1, after 2 iterations. Modified compensators k_1 and k_2, $v_x = 14m/s$. Second order actuator.

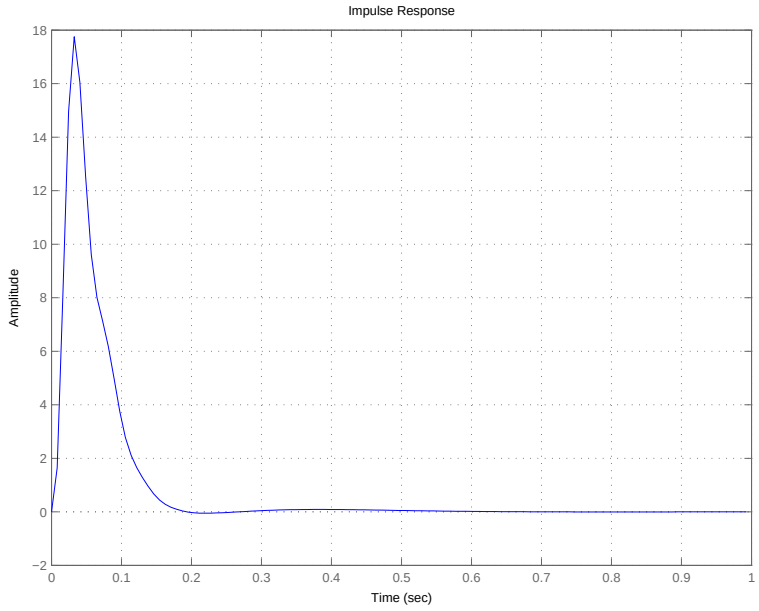

Figure 5.17: Impulse response of C_2, after 2 iterations. Modified compensators k_1 and k_2, $v_x = 14m/s$. Second order actuator.

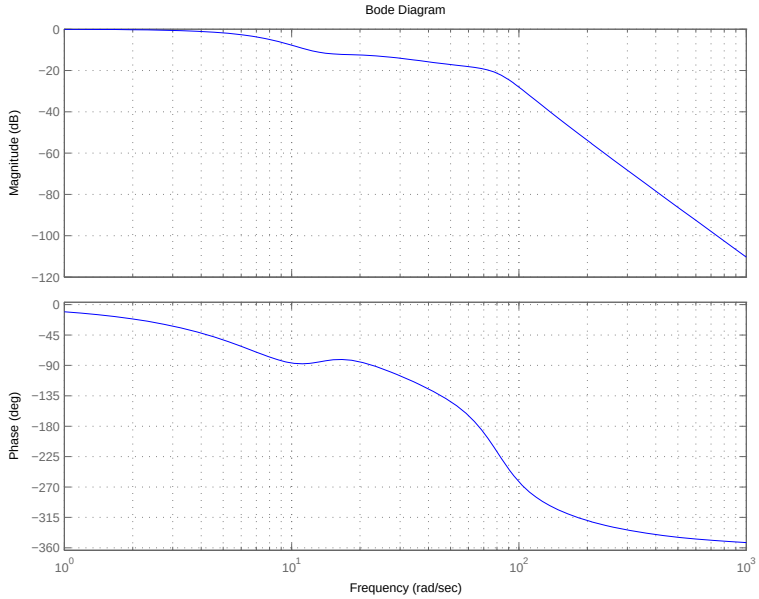

Figure 5.18: Bode plot of first loop closed with modified compensators k_1 and k_2 after 2 iterations.

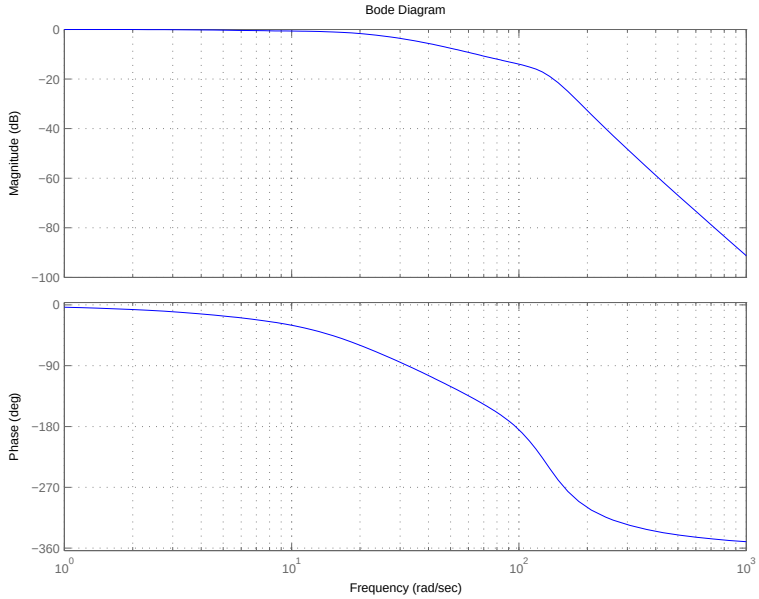

Figure 5.19: Bode plot of second loop closed with modified compensators k_1 and k_2 after 2 iterations.

Table 5.3: Gain, and complex zero pair, of the two compensators with second order actuator and $v_x = 14$.

	Gain K_i $(i = 1, 2)$	**Zero** z_i $(i = 1, 2)$
Channel C_1	0.5964	$-5.1780 + 14.1772i$
Channel C_2	-5.8253	$-5.1780 + 14.1772i$

Table 5.4: Phase margin and crossover frequency of both channels, with second order actuator and $v_x = 14$. Modified compensators.

	Phase margin, $\Delta\phi$	**Cross-over frequency** (rad/s)
Channel C_1	76°	4.98
Channel C_2	72°	18.1

ality is shown to be very sensitive to changes in tyre parameters. A notch filter can be used with the first compensator to get rid of the plateau, and a higher bandwidth might then be allowed. An additional complex pole pair, in addition to the complex zero pair already used, has been tried out. This would pull the lightly damped complex pole pair towards the left in the complex plane and increase the damping of that pole. However, the open loop phase margin would decrease significantly, with a resulting loss in robustness, which has been proved in simulations.

5.1 Controller Scheduling

The design in the previous section was made with speed 14 m/s, by placing a zero right on the most lightly damped pole of the open system. But, the system must have the same closed loop characteristics for all speeds that can be reached with normal driving. The bandwidth has to be maintained and phase margin has to remain above the specified value. Too low speeds do not cause any need for feedback, and the interesting speeds in this case are from 5 m/s to 30 m/s. Figure 5.20 shows how the most lightly damped pole

varies with longitudinal speed.

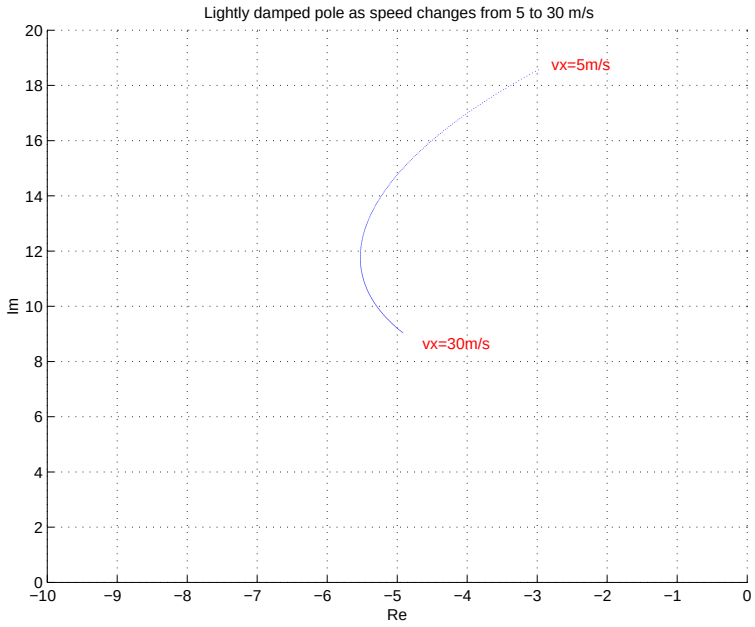

Figure 5.20: Most lightly damped open loop pole as a function of speed

This implies that the compensators have to be adapted continuously with respect to speed. First, the complex zero pair must be placed on the lightly damped pole, according to figure 5.20. Then, a gain scheduling has to be done to obtain the specified crossover frequency (5 rad/s for channel 1 and 18 rad /s for channel 2). The transfer function of the first channel, C_1, is calculated. Since the bandwidth of channel 1 is small in comparison to channel 2, the transfer function h_2 can be set to 1, and C_1 can easily be calculated. Now, the gain at the desired crossover frequency, i.e. 5 rad/s, is evaluated, and inverted, which will give the correct gain of the first compensator. Once this compensator is determined, h_1 and C_2 can easily be calculated. The gain at 18 rad/s is evaluated, and an inversion will give the gain of the second compensator. How the scheduling is carried out in practice is shown in the appendix.

Figures 5.21 to 5.36 show the root locus plots, bode plots, step and impulse responses, for both channels, and for speeds 10 m/s and 25 m/s, after following the above mentioned scheduling procedure. In figure 5.37, the bode plot of the first channel, with speeds between 5 m/s to 25 m/s, is illustrated. For lower speeds, the roll-off around the frequencies of the controller zero is considerably higher than for high speeds. Furthermore, a higher gain margin is also observed for low speeds. This means that the system shows a much

better noise rejection for low than for high speeds. On the other hand, the phase margin decreases for lower speeds, as shown in table 5.5. This results in lower damping and a more oscillatory behaviour, which is never an issue for high speeds. For the second channel, the behaviour is rather similar for all speeds (figure 5.38), and, above all, much faster than for the first channel, mainly due to the higher gain giving a higher crossover frequency. In general, the system seems to have a faster behaviour for low speeds, but also a larger settling time, which can be seen in the closed loop step and impulse responses in figures 5.39 to 5.42. The faster and more oscillatory characteristics for low speeds can be explained by studying the root-locus plot of the first channel, for a low and a high speed respectively, as in figures 5.21 and 5.29. For the lower speed (10 m/s, fig. 5.21), a not completely out-cancelled pole with damping 0.5 is present, while for the higher speed (25 m/s, fig. 5.29), the damping is much greater, 0.8. The actuator pole is badly damped, but its high frequency makes the impact on the channel negligible.

The specifications that were put up for phase margin, are, as can be seen in table 5.5, precisely met. The specified step response and impulse noise rejection settling time of 0.5 s, is, according to figures 5.39 to 5.42, reached for both channels (the definition of settling time can be found in the litterature). However, the settling time is much longer for channel 1.

Table 5.5: Phase margin of both channels, with second order actuator, and for different speeds. Modified compensators.

	25 m/s	**21 m/s**	**18 m/s**	**14 m/s**	**10 m/s**	**5 m/s**
Channel C_1	92.4°	85.1°	80.6°	75.8°	73.9°	76.5°
Channel C_2	79.7°	75.6°	73.7°	71.7°	71.4°	72.2°

5.2 System Integrity and Robustness

In this section, system integrity and robustness to plant uncertainties are studied. We recall from section 4.3 that determining system integrity is done by inspection of the poles of C_1 and C_2.

1. Figure 5.1 shows that the plant transfer matrix has no right half plane poles. These poles are equivalent to the poles of the individual plant transfer functions $g_{ij}(s)$, $i, j = 1, 2$ [Maciejowski].

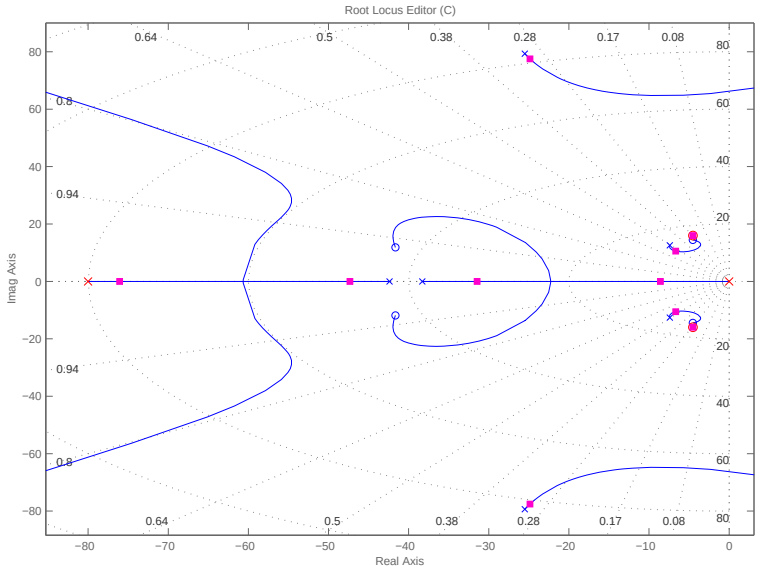

Figure 5.21: Channel 1 closed after 2 iterations. Modified compensators k_1 and k_2, $v_x = 10m/s$. Second order actuator.

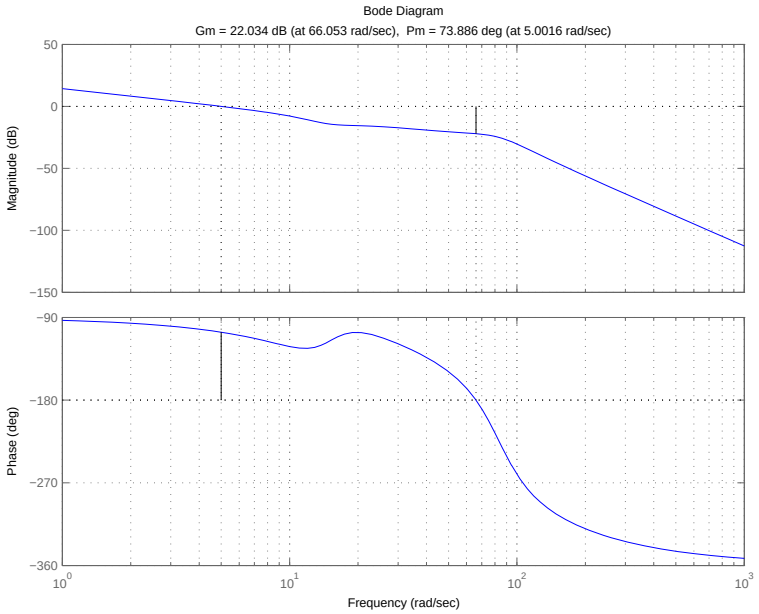

Figure 5.22: Bode plot of channel 1 with modified compensators k_1 and k_2 after 2 iterations. $v_x = 10m/s$.

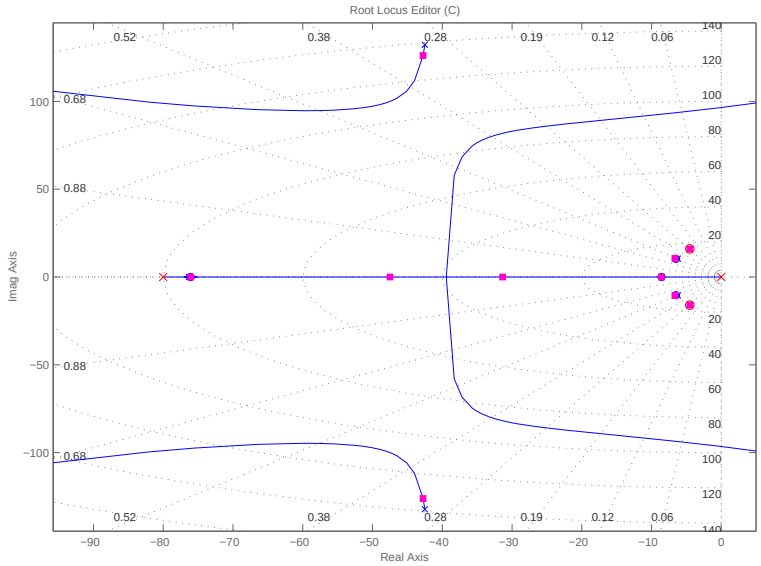

Figure 5.23: Channel 2 closed after 2 iterations. Modified compensators k_1 and k_2, $v_x = 10m/s$. Second order actuator.

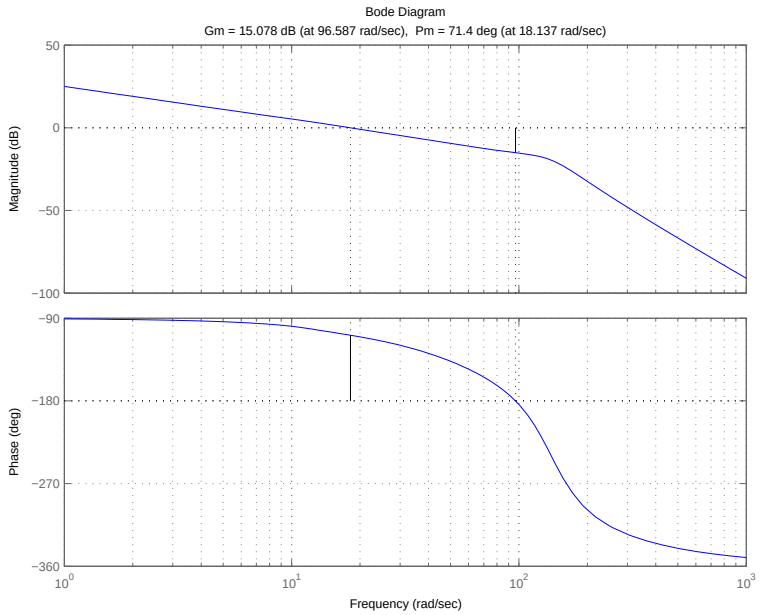

Figure 5.24: Bode plot of channel 2 with modified compensators k_1 and k_2 after 2 iterations. $v_x = 10m/s$.

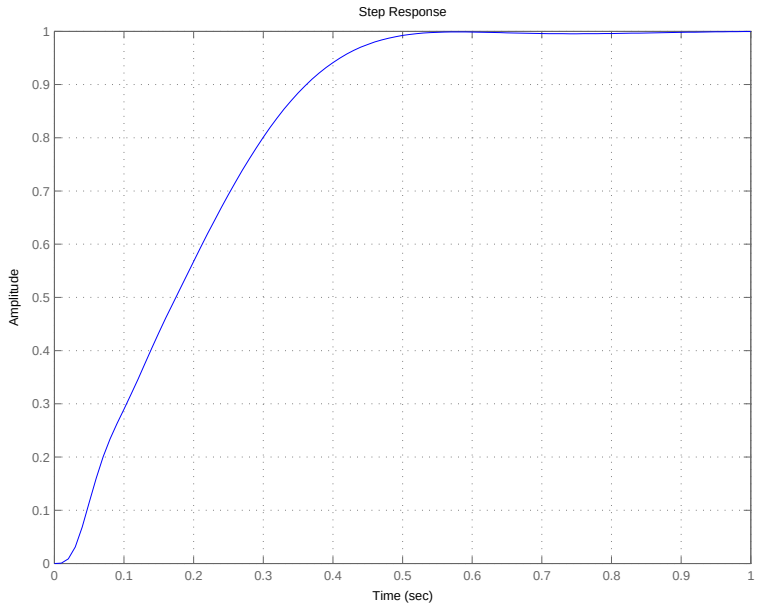

Figure 5.25: Step response of C_1, after 2 iterations. Modified compensators k_1 and k_2, $v_x = 10m/s$. Second order actuator.

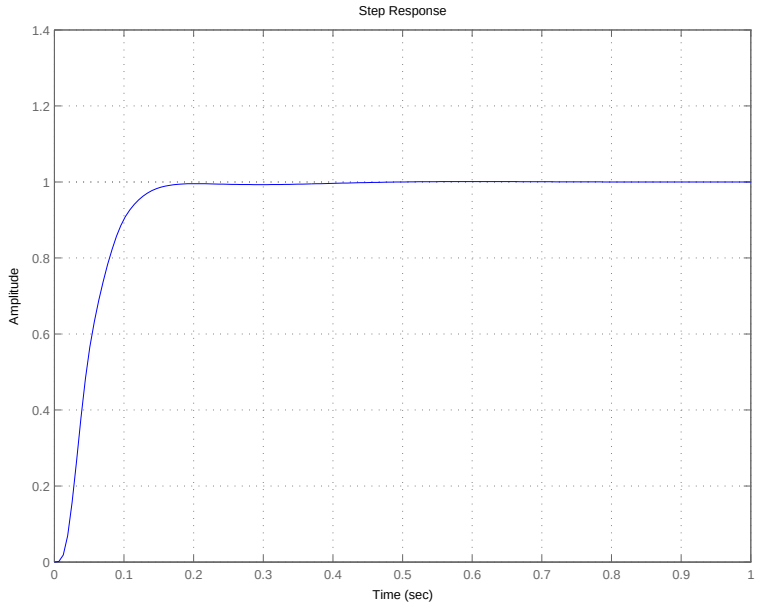

Figure 5.26: Step response of C_2, after 2 iterations. Modified compensators k_1 and k_2, $v_x = 10m/s$. Second order actuator.

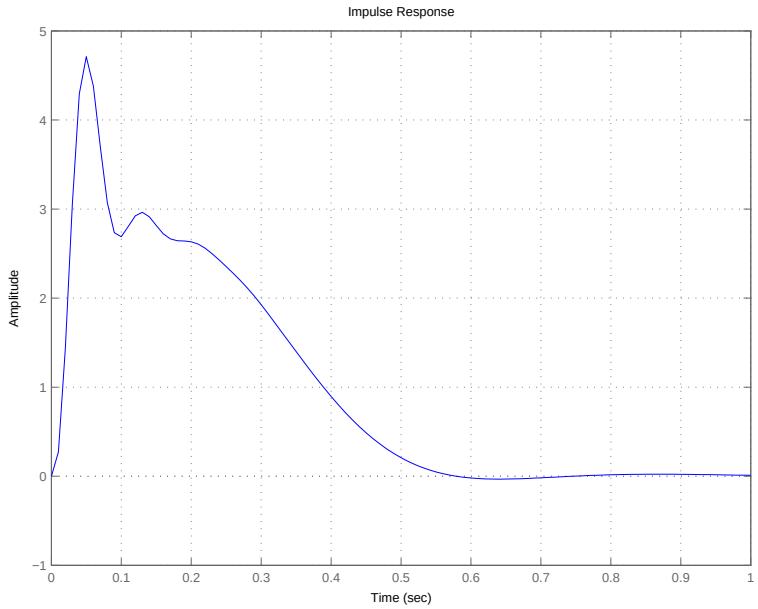

Figure 5.27: Impulse response of C_1, after 2 iterations. Modified compensators k_1 and k_2, $v_x = 10m/s$. Second order actuator.

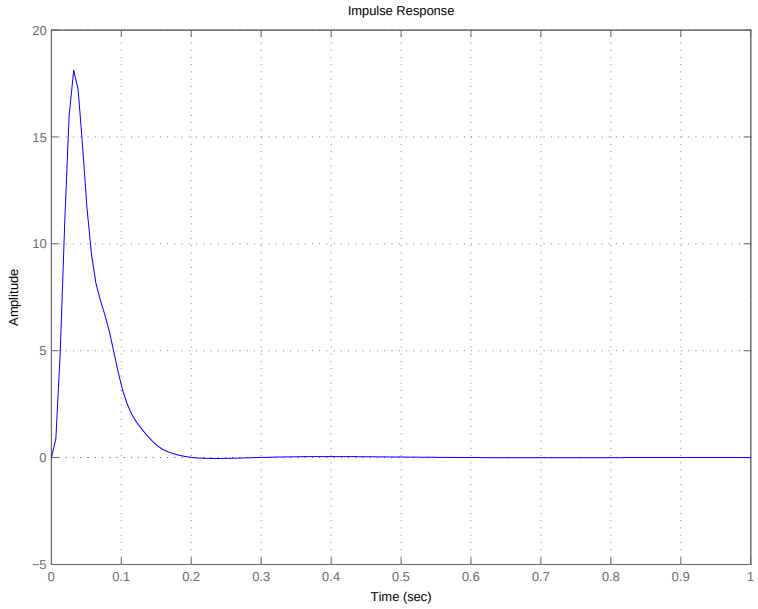

Figure 5.28: Impulse response of C_2, after 2 iterations. Modified compensators k_1 and k_2, $v_x = 10m/s$. Second order actuator.

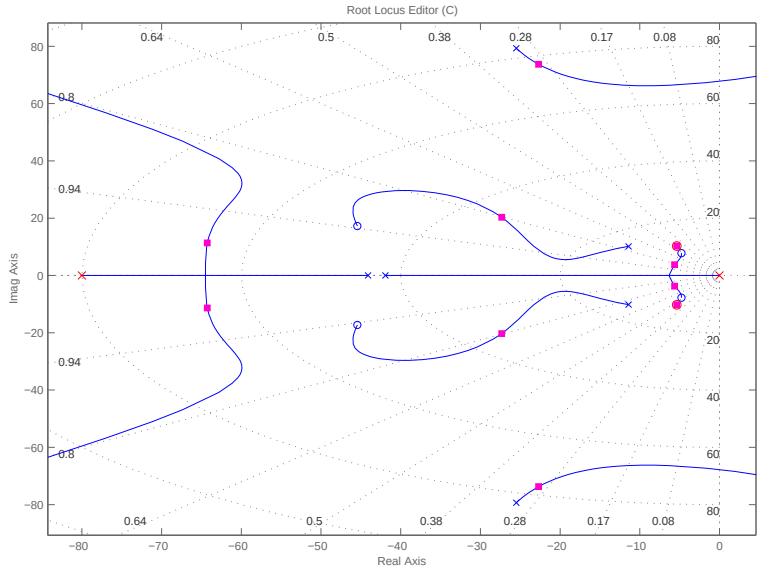

Figure 5.29: Channel 1 closed after 2 iterations. Modified compensators k_1 and k_2, $v_x = 25m/s$. Second order actuator.

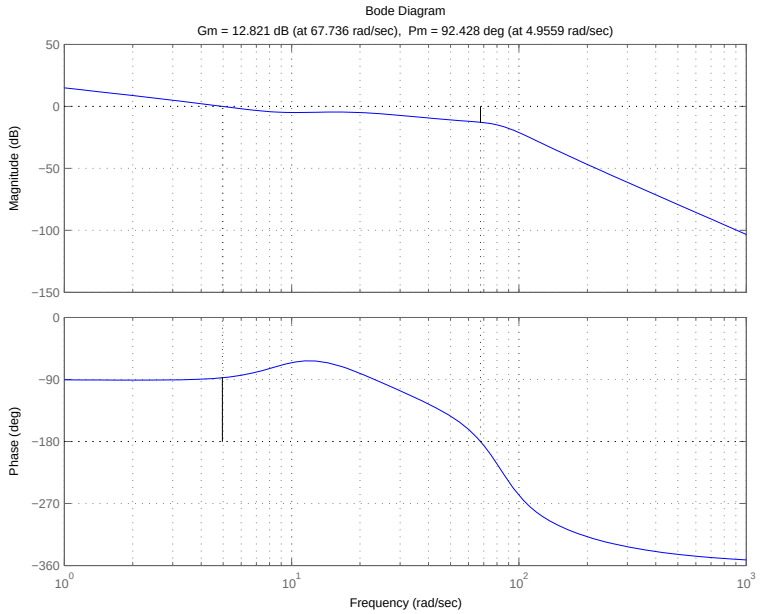

Figure 5.30: Bode plot of channel 1 with modified compensators k_1 and k_2 after 2 iterations. $v_x = 25m/s$.

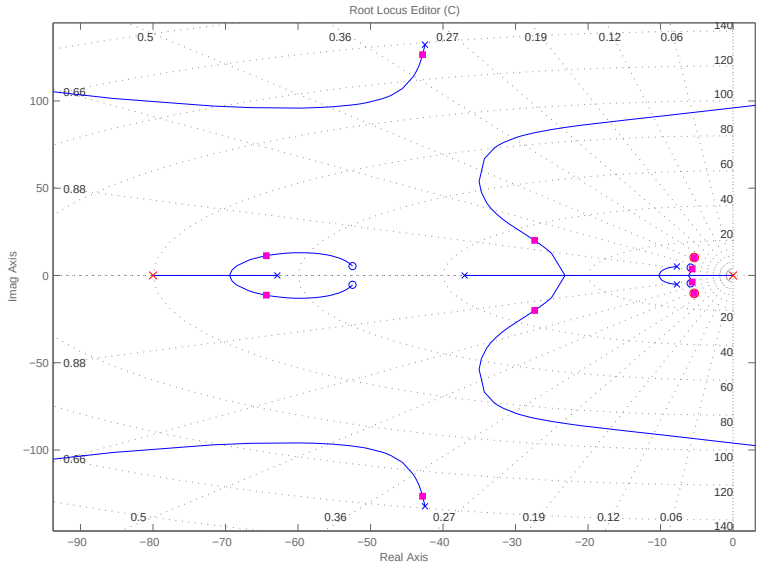

Figure 5.31: Channel 2 closed after 2 iterations. Modified compensators k_1 and k_2, $v_x = 25m/s$. Second order actuator.

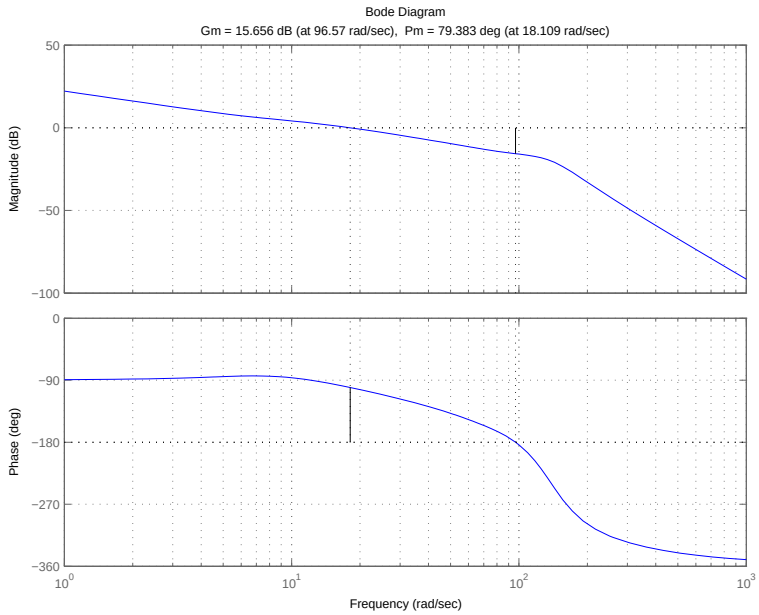

Figure 5.32: Bode plot of channel 2 with modified compensators k_1 and k_2 after 2 iterations. $v_x = 25m/s$.

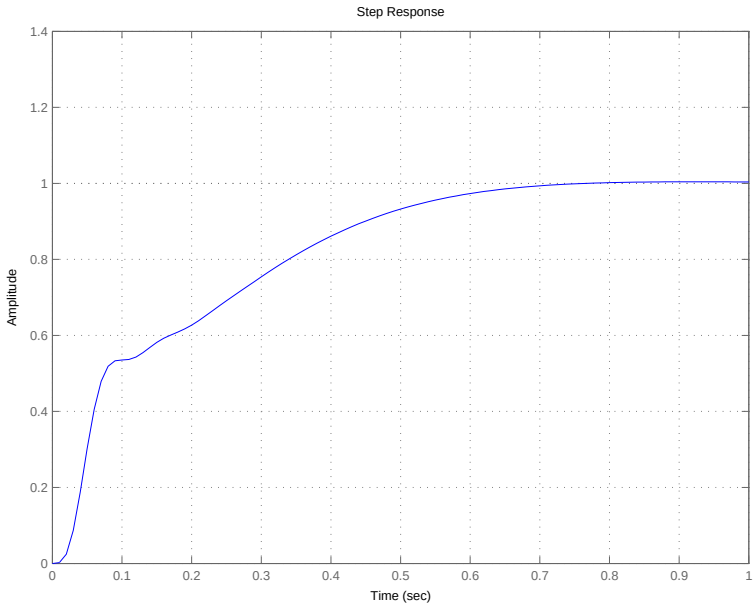

Figure 5.33: Step response of C_1, after 2 iterations. Modified compensators k_1 and k_2, $v_x = 25m/s$. Second order actuator.

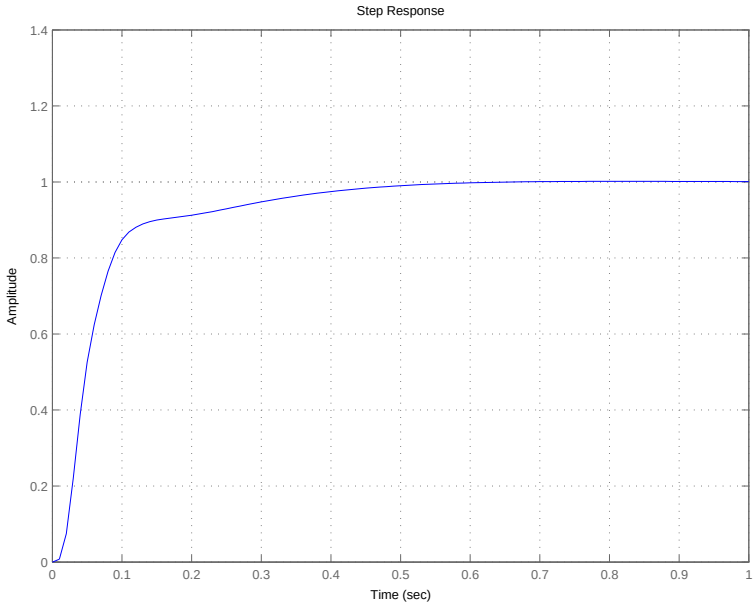

Figure 5.34: Step response of C_2, after 2 iterations. Modified compensators k_1 and k_2, $v_x = 25m/s$. Second order actuator.

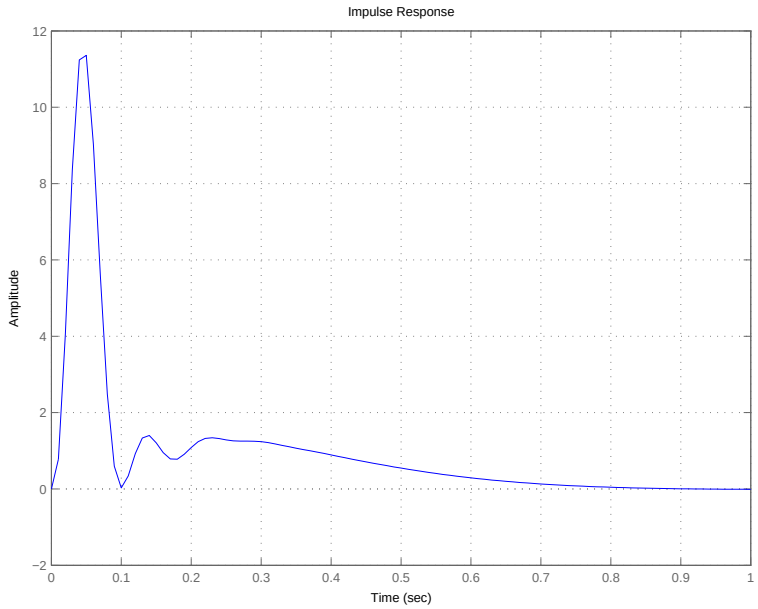

Figure 5.35: Impulse response of C_1, after 2 iterations. Modified compensators k_1 and k_2, $v_x = 25m/s$. Second order actuator.

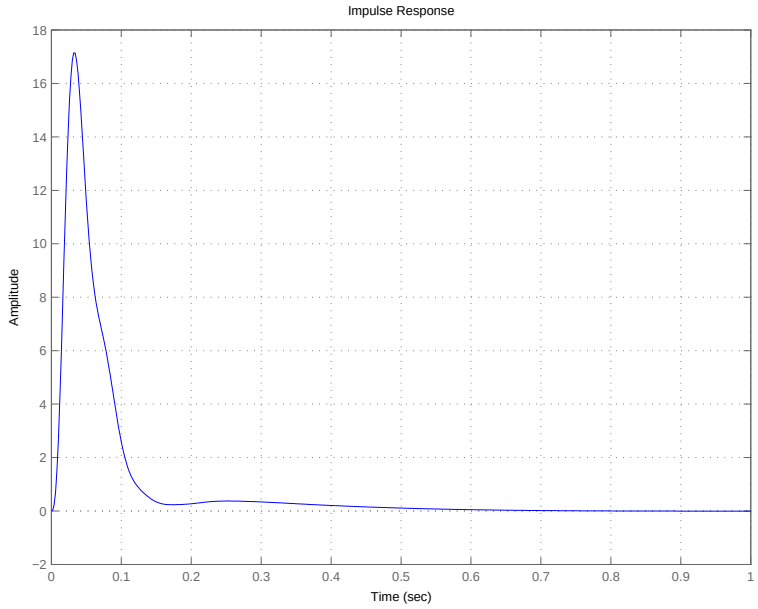

Figure 5.36: Impulse response of C_2, after 2 iterations. Modified compensators k_1 and k_2, $v_x = 25m/s$. Second order actuator.

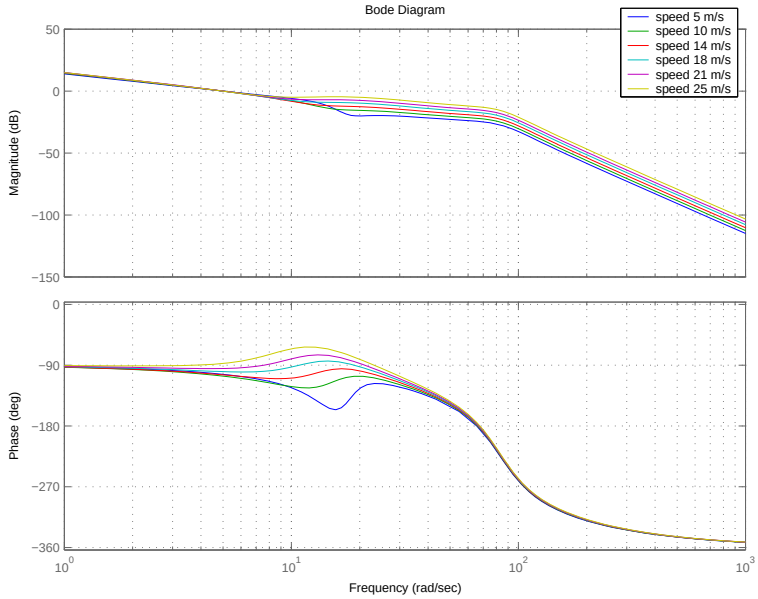

Figure 5.37: Bode plot of channel 1 for different speeds with modified compensators k_1 and k_2 after 2 iterations.

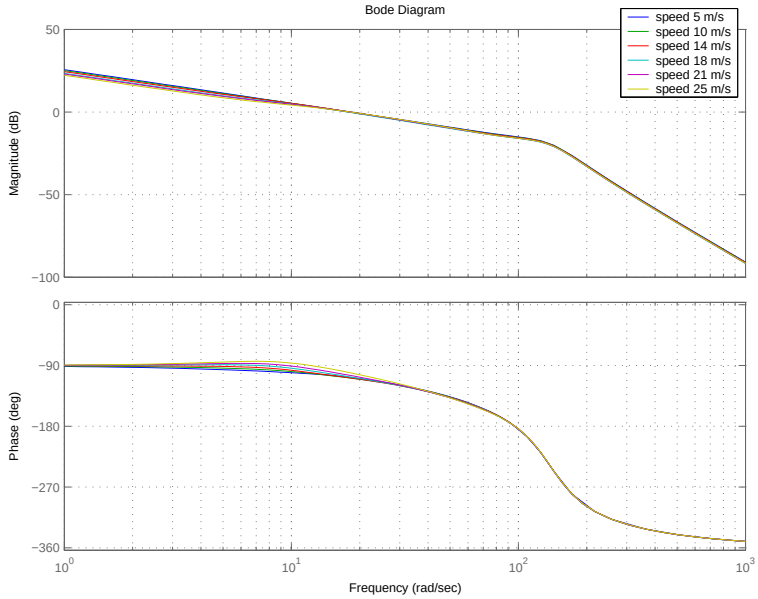

Figure 5.38: Bode plot of channel 2 for different speeds with modified compensators k_1 and k_2 after 2 iterations.

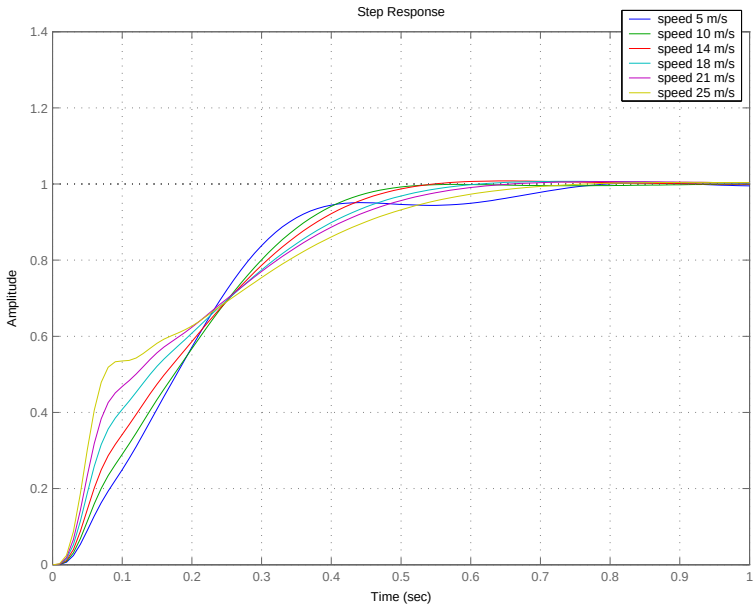

Figure 5.39: Step response of C_1, after 2 iterations, for different speeds. Modified compensators k_1 and k_2. Second order actuator.

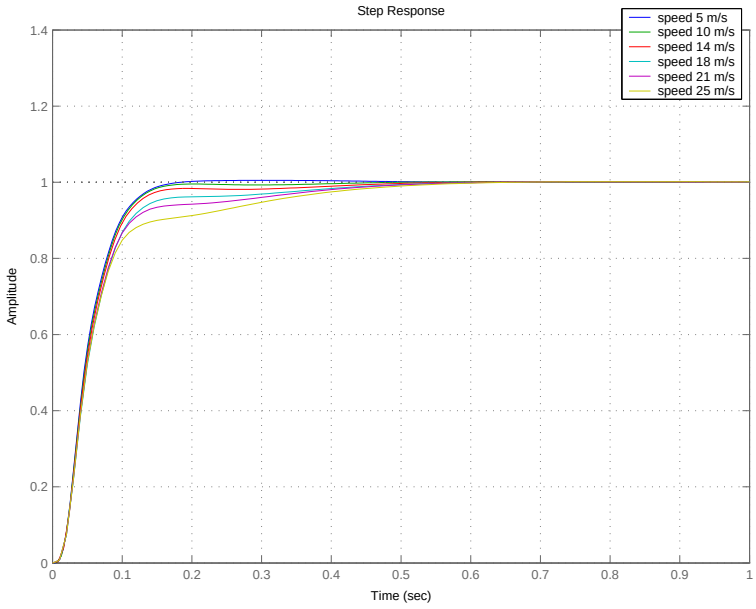

Figure 5.40: Step response of C_2, after 2 iterations, for different speeds. Modified compensators k_1 and k_2. Second order actuator.

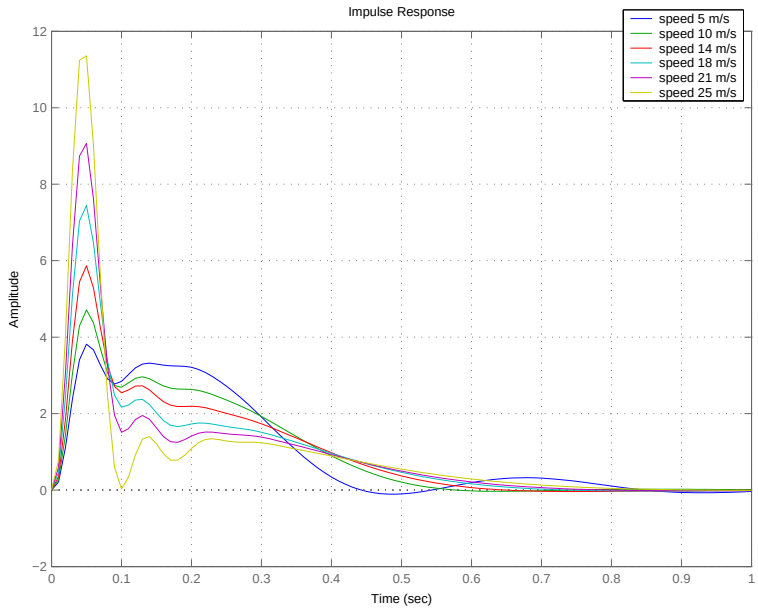

Figure 5.41: Impulse response of C_1, after 2 iterations, for different speeds. Modified compensators k_1 and k_2. Second order actuator.

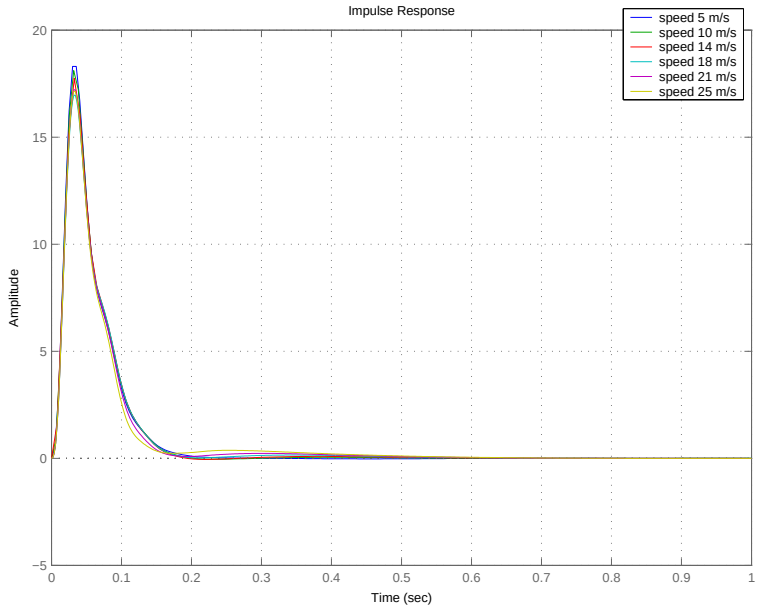

Figure 5.42: Impulse response of C_2, after 2 iterations, for different speeds. Modified compensators k_1 and k_2. Second order actuator.

2. The bode plots of $k_1 g_{11}$ and $k_2 g_{22}$, for speeds between 5 m/s and 25 m/s, are shown in figures 5.43 and 5.44. The phase margin is well above $-180°$, which proves the stability of h_1 and h_2.

Similarly, the requirements for robustness from section 4.3 are checked:

1. The phase margins from table 5.5 do not fall below the specified value.

2. Figures 5.45 and 5.46 show Nyquist plots of γh_1 and γh_2, for frequencies up to the crossover frequency. Neither of them goes close to the point (1,0).

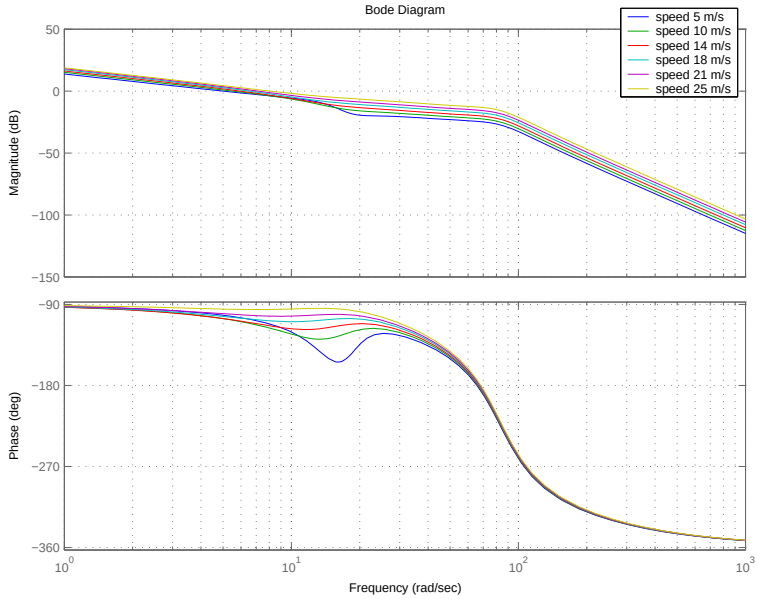

Figure 5.43: Bode plot of channel 1, for different speeds, with modified compensators k_1 and k_2 after 2 iterations. Second loop broken.

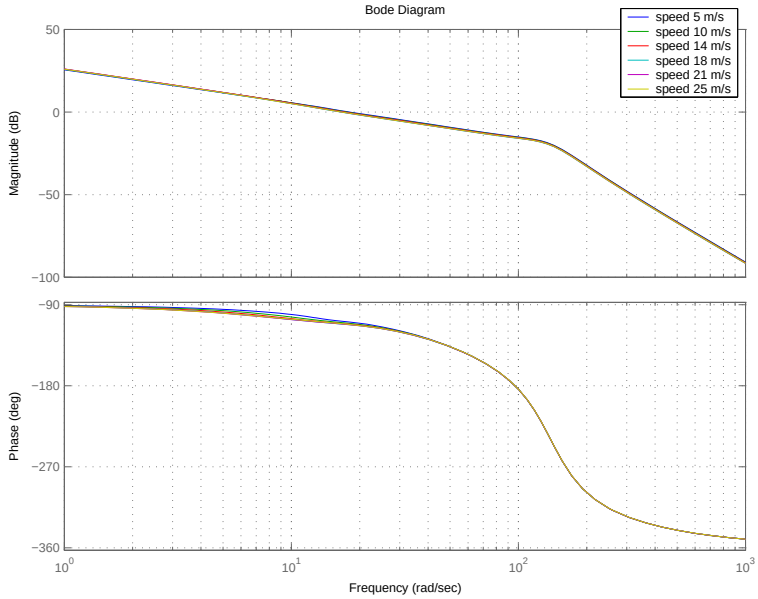

Figure 5.44: Bode plot of channel 2, for different speeds, with modified compensators k_1 and k_2 after 2 iterations. First loop broken.

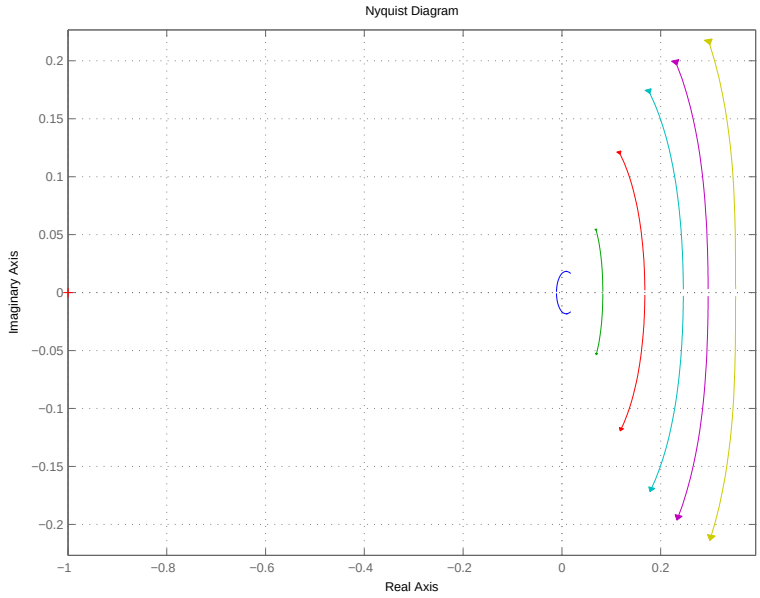

Figure 5.45: Nyquist plot of γh_1 for frequencies up to 6 rad/s, and for increasing speed from left to right. Modified compensators k_1 and k_2. Second order actuator.

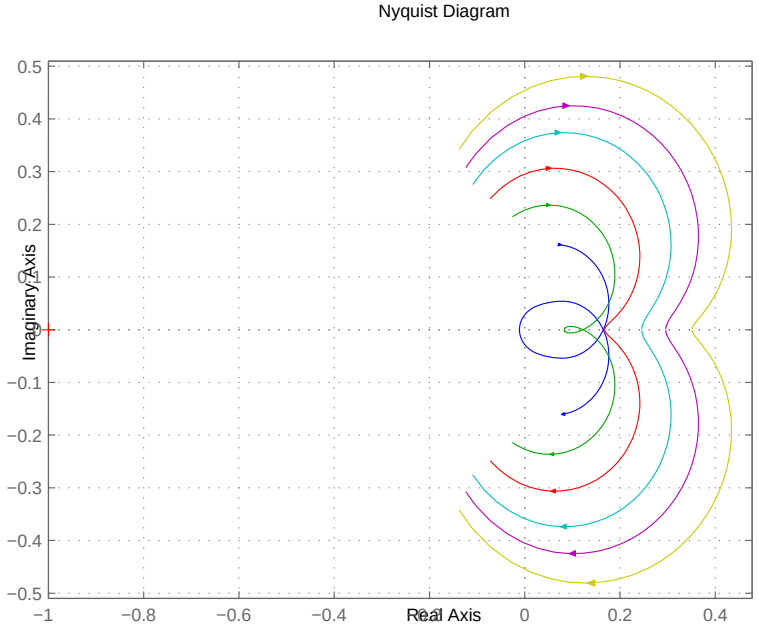

Figure 5.46: Nyquist plot of γh_2 for frequencies up to 20 rad/s, and for increasing speed from left to right. Modified compensators k_1 and k_2. Second order actuator.

6 Simulation Results

In this section, small signal behaviour of the feedback control will be studied. Simulations are carried out, first on the simple linear one-track model used for the design, and later on a nonlinear and more realistic complete 4 wheel steering vehicle model. Robustness and system integrity of the design will be tested by applying a 20 ms time delay and breaking one of the control loops. A small impulse disturbance will be used to check the disturbance rejection.

The model that is used for simulation has 4 wheel steering and all the nonlinear dynamics present in a real vehicle. It is programmed in C, with an interface to Matlab Simulink. Inputs to the model are front and rear wheel steering angles, brake torque, surface parameters such as slope and friction coefficients, and drive train torque. All outputs are measurable states. The outputs are the lateral and longitudinal acceleration, rotational wheel speeds, and the yaw rate. The lateral and longitudinal velocities, needed to calculate the side slip angle, are observable states and are kept in a logged output. A controller for longitudinal speed is needed to prevent the speed from dropping while making a turning manoeuvre.

Figures 6.1 to 6.14 show simulations after using the control design and scheduling from chapter 5. A lowpass filtered step reference of 0.1 rad/s ($5.7°/s$) for yaw rate, and a small impulse disturbance 1 second after the step, are used, beyond trying to keep the side slip angle as small as possible (constant reference of 0 radians). From these figures, a decreasing peak of the side slip angle, as the speed decreases, can be observed. Beyond that, the observations from section 5.1 are confirmed; for low speeds, on the linear model, there it a more oscillatory behaviour. This is not so evident on the complete model, probably because of smaller gain or more damping.

6.1 Introducing Time Delay

The control system is designed with enough phase margin to handle a 20 ms time delay. But, its robustness has to be proved, and, even with plant uncertainties, it has to behave in a satisfactory manner. This is shown in figures 6.15 to 6.28. In general, the yaw rate step response has slightly more overshoot than in the case without time delay. Similarly, the peak of the side slip angle is larger than in the previous case. The jagged behaviour that can be seen for high speed, in figure 6.15, can be compensated for by the feedforward. Figures 6.29 and 6.30 show the simulations for speeds between 5 and 25 m/s.

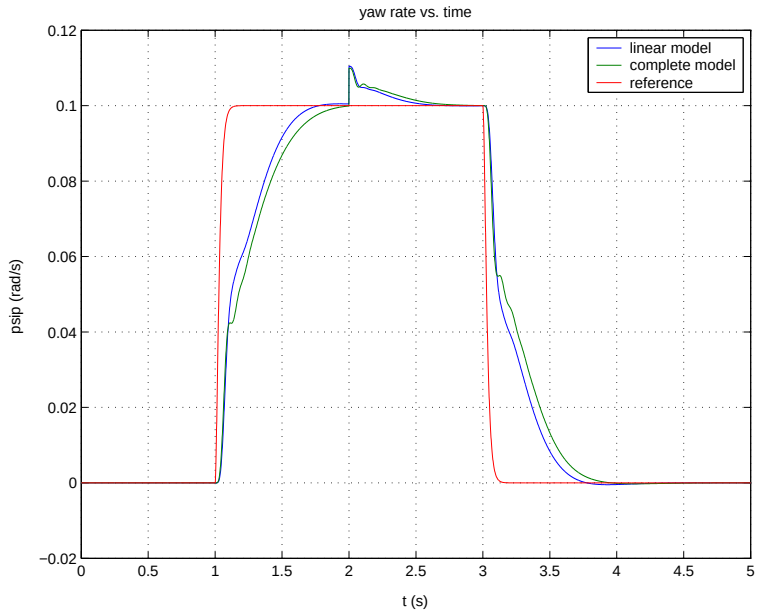

Figure 6.1: Simulation on model with second order actuator, $v_x = 25m/s$.

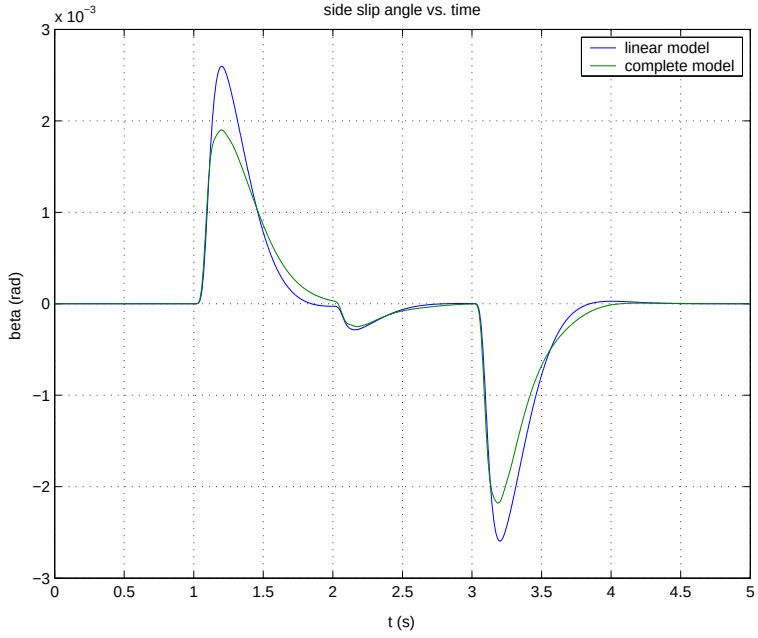

Figure 6.2: Simulation on model with second order actuator, $v_x = 25m/s$. Side slip angle β_r.

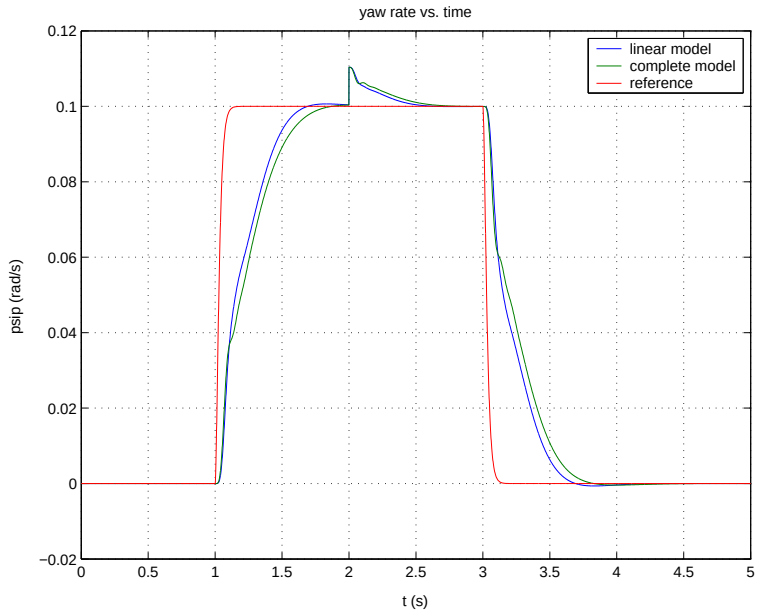

Figure 6.3: Simulation on model with second order actuator, $v_x = 21m/s$.

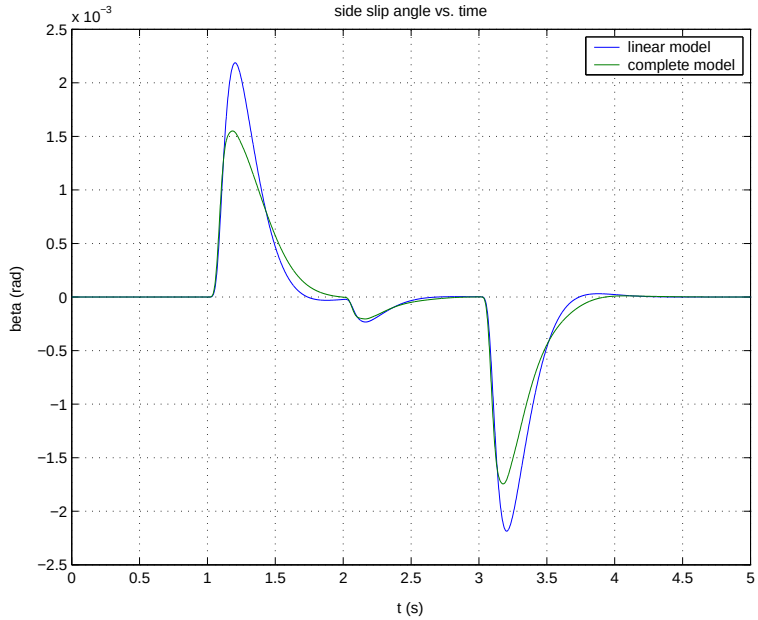

Figure 6.4: Simulation on model with second order actuator, $v_x = 21m/s$. Side slip angle β_r.

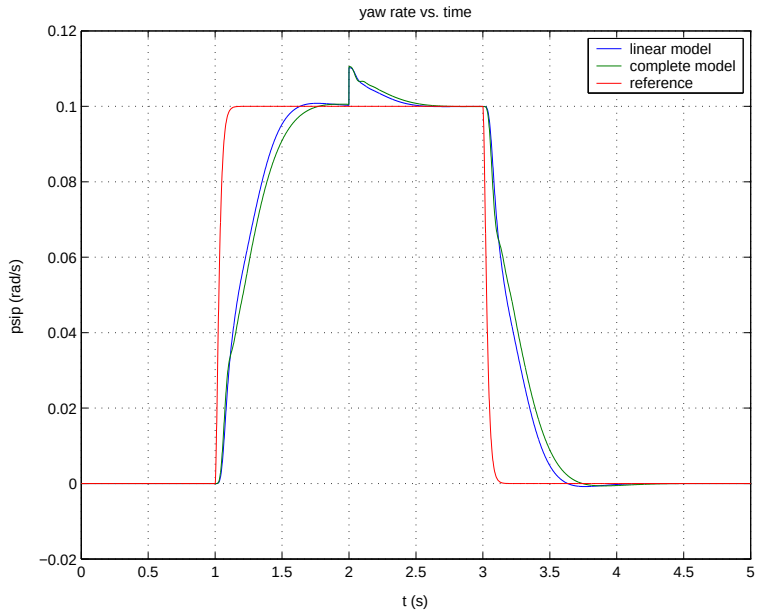

Figure 6.5: Simulation on model with second order actuator, $v_x = 18m/s$.

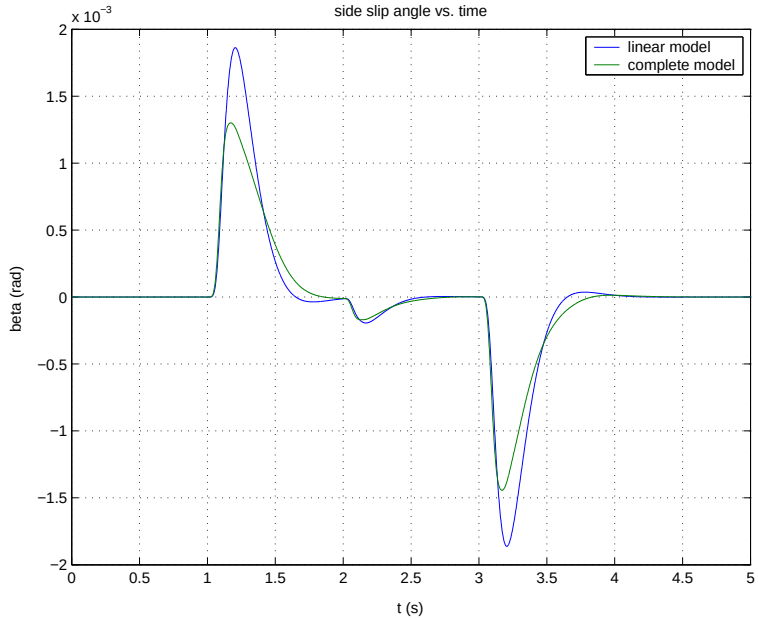

Figure 6.6: Simulation on model with second order actuator, $v_x = 18m/s$. Side slip angle β_r.

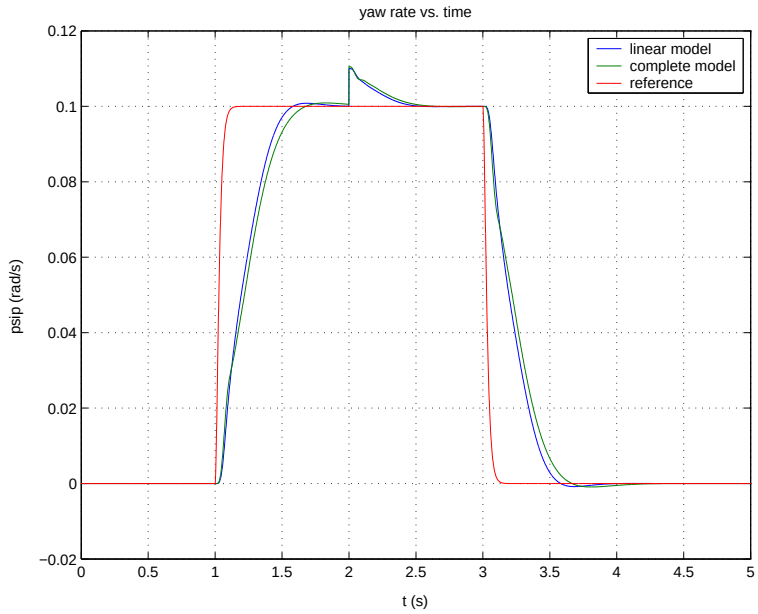

Figure 6.7: Simulation on model with second order actuator, $v_x = 14m/s$.

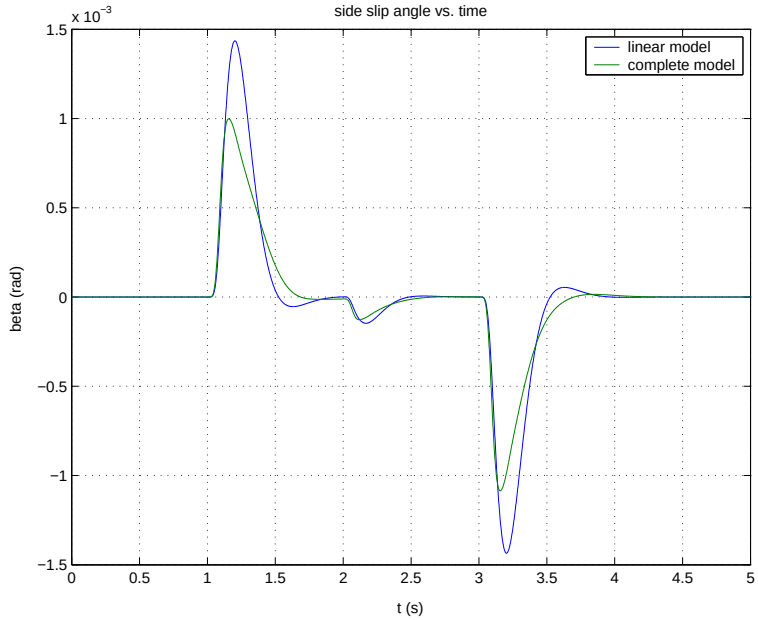

Figure 6.8: Simulation on model with second order actuator, $v_x = 14m/s$. Side slip angle β_r.

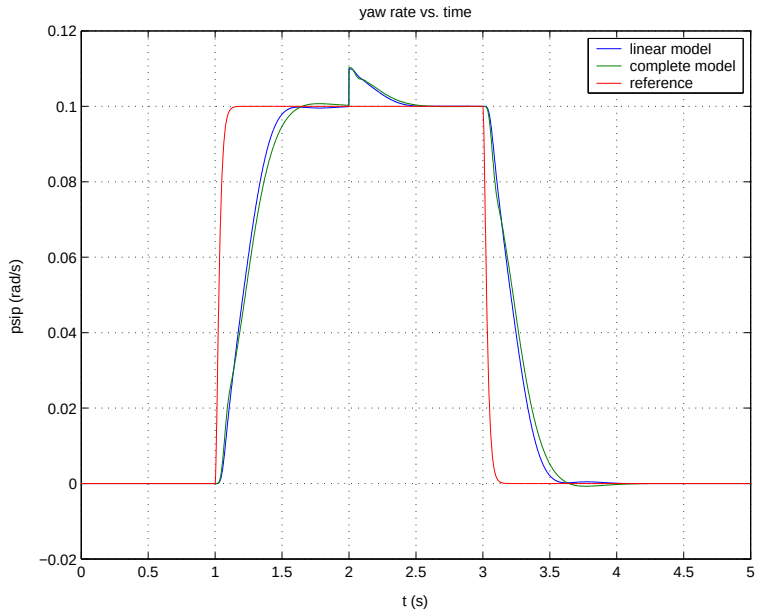

Figure 6.9: Simulation on model with second order actuator, $v_x = 10m/s$.

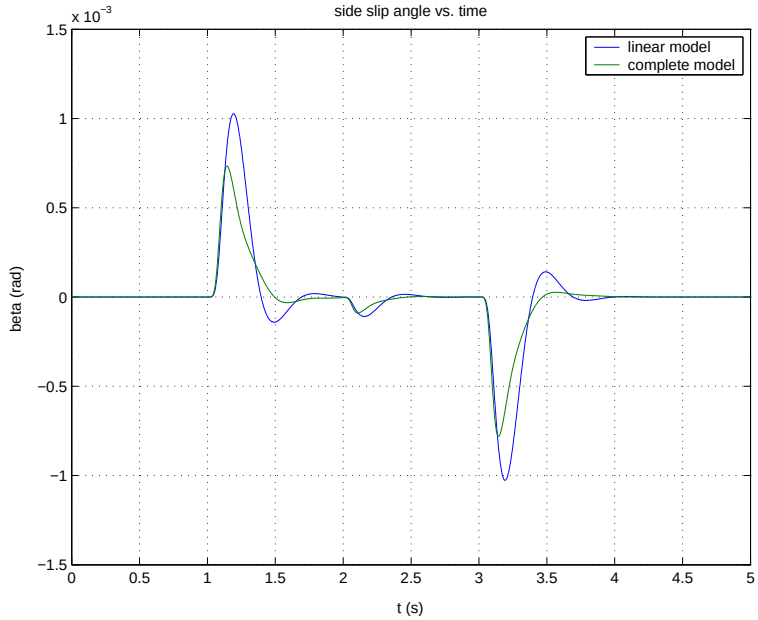

Figure 6.10: Simulation on model with second order actuator, $v_x = 10m/s$. Side slip angle β_r.

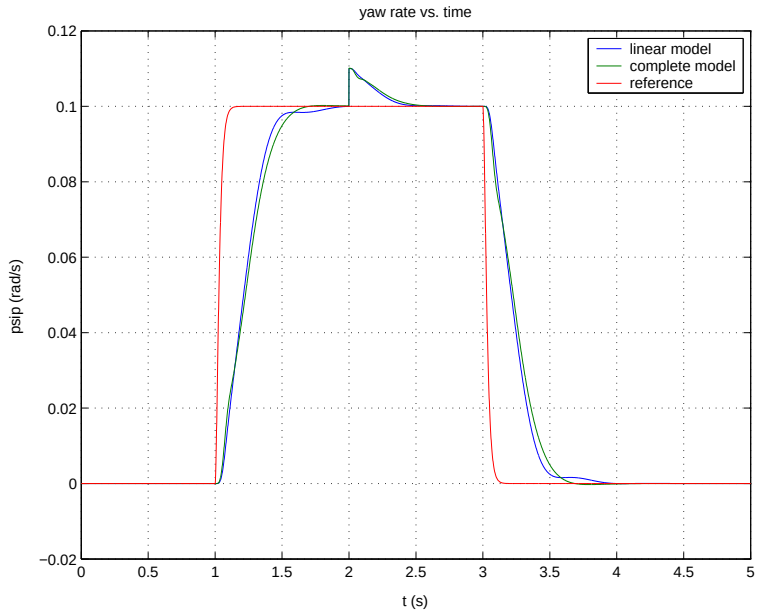

Figure 6.11: Simulation on model with second order actuator, $v_x = 8m/s$.

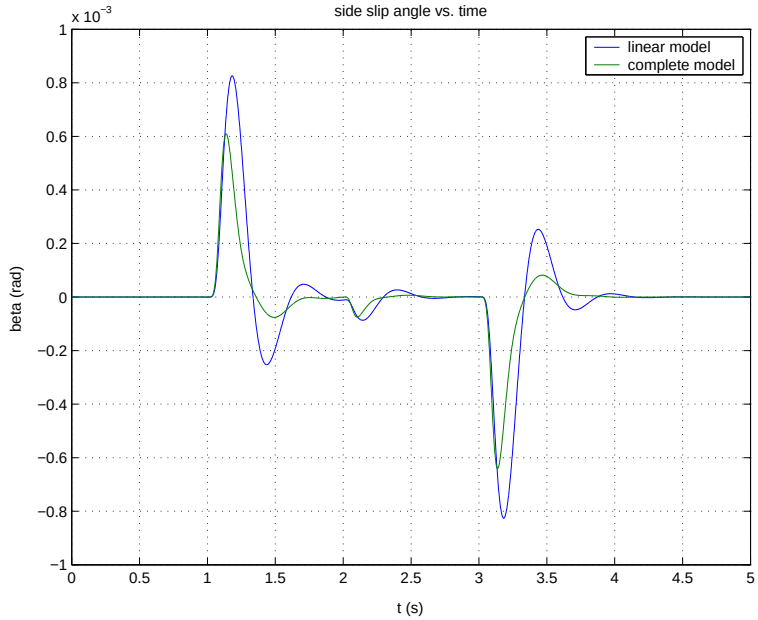

Figure 6.12: Simulation on model with second order actuator, $v_x = 8m/s$. Side slip angle β_r.

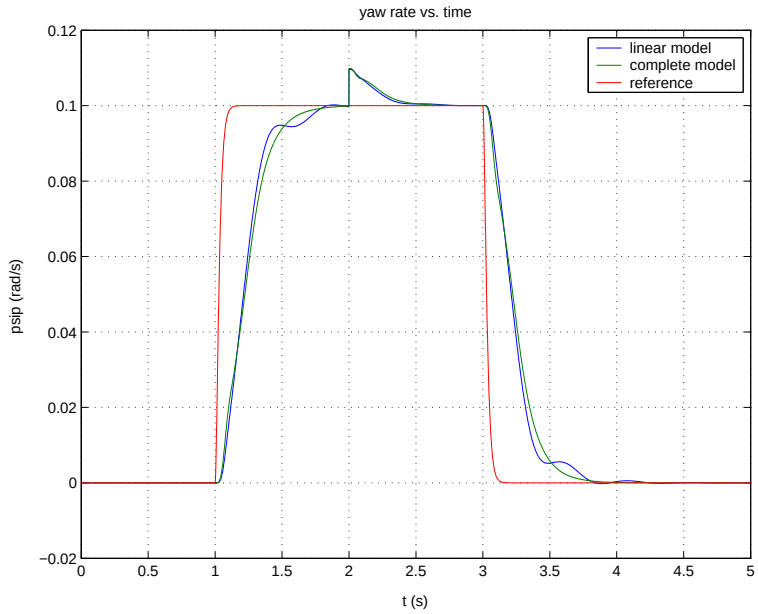

Figure 6.13: Simulation on model with second order actuator, $v_x = 5m/s$.

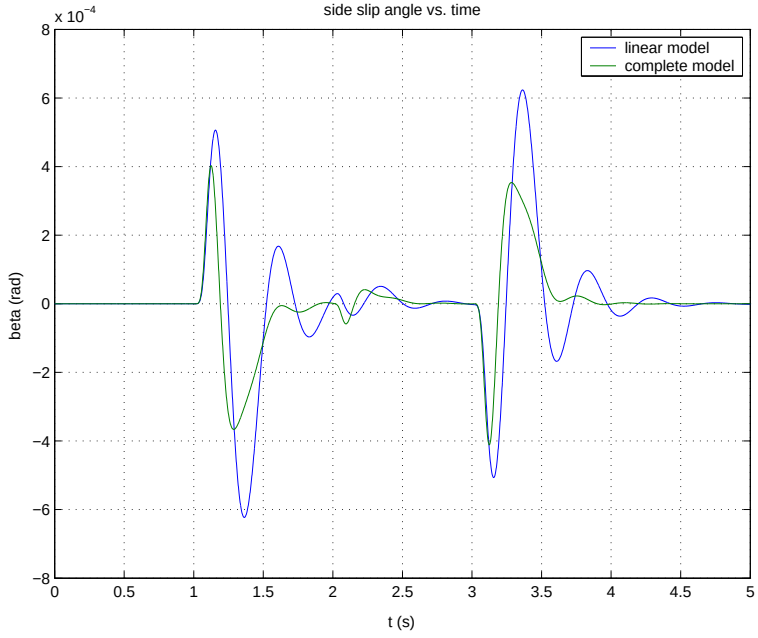

Figure 6.14: Simulation on model with second order actuator, $v_x = 5m/s$. Side slip angle β_r.

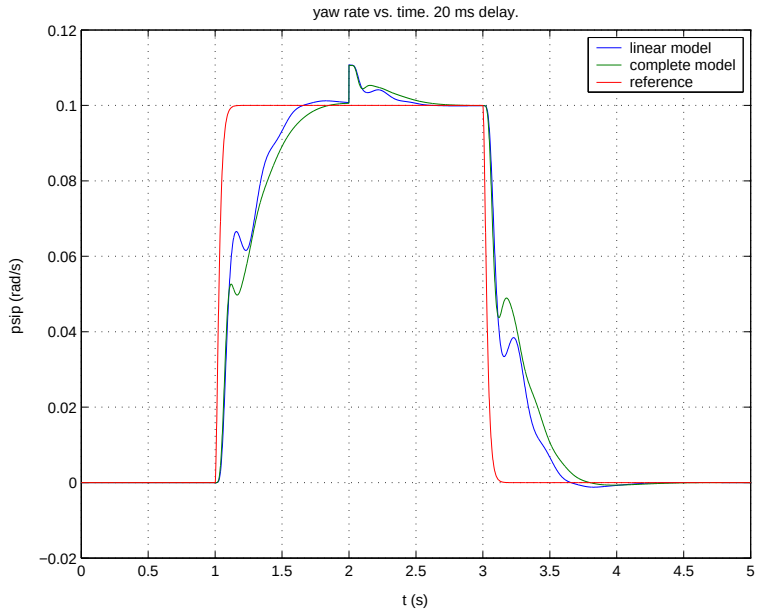

Figure 6.15: Simulation on model with second order actuator, $v_x = 25m/s$. Time delay 20 ms.

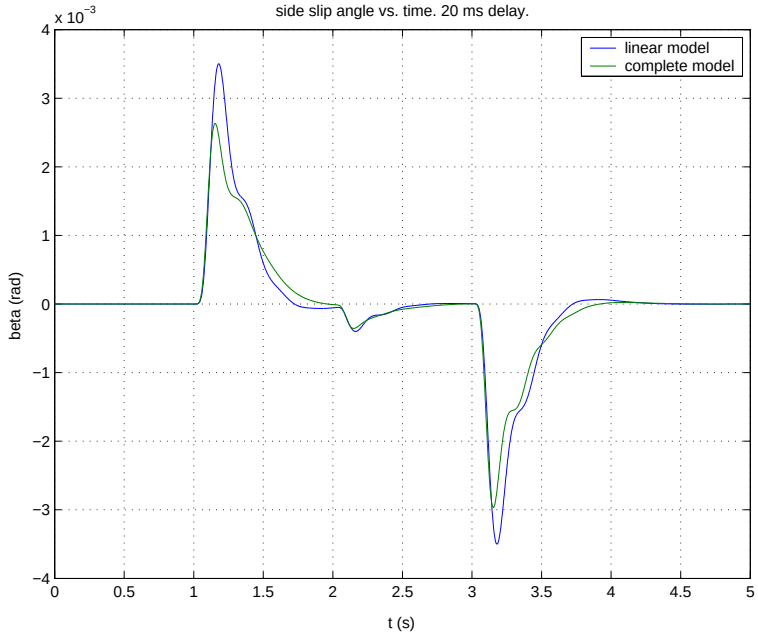

Figure 6.16: Simulation on model with second order actuator, $v_x = 25m/s$. Side slip angle β_r. Time delay 20 ms.

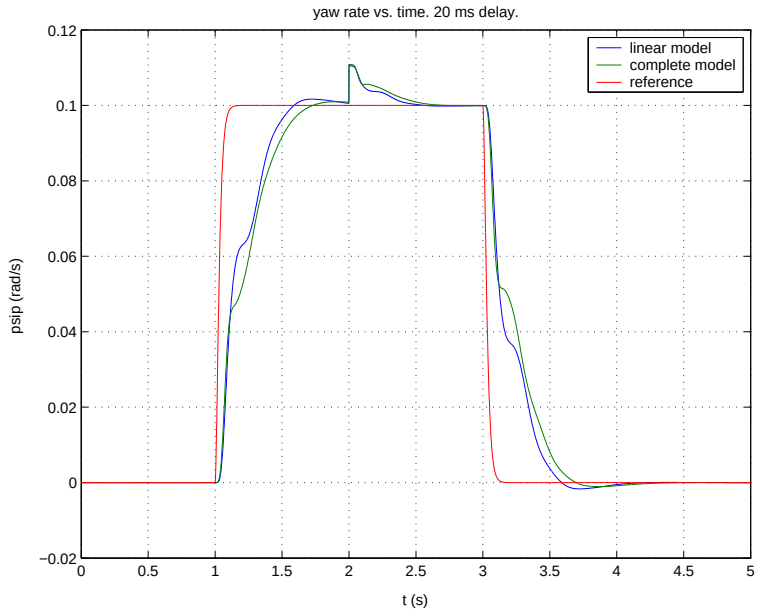

Figure 6.17: Simulation on model with second order actuator, $v_x = 21m/s$. Time delay 20 ms.

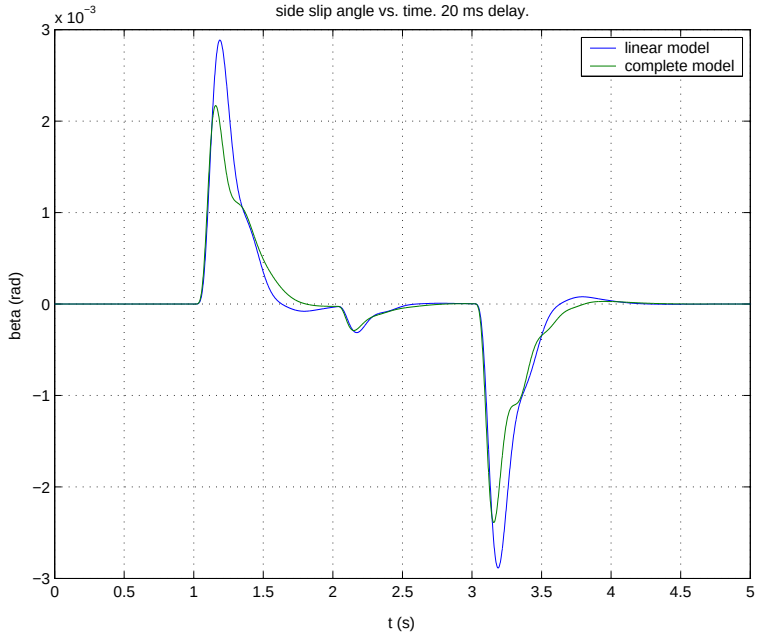

Figure 6.18: Simulation on model with second order actuator, $v_x = 21m/s$. Side slip angle β_r. Time delay 20 ms.

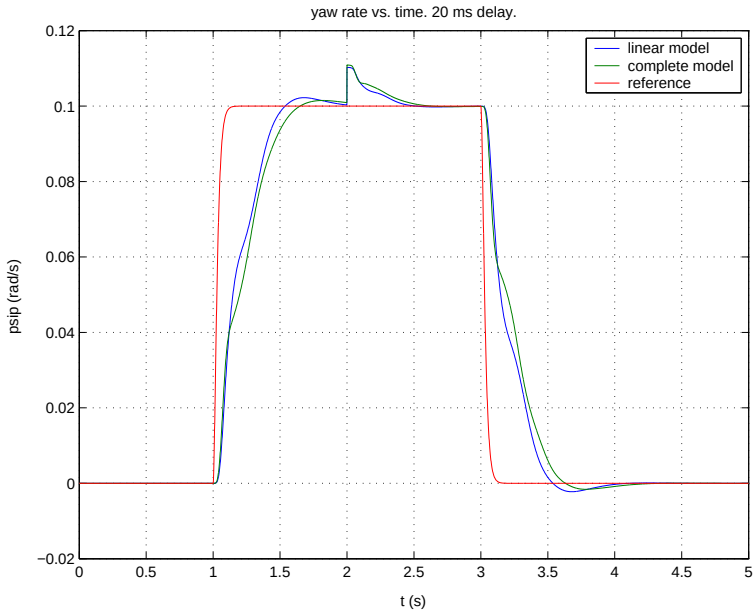

Figure 6.19: Simulation on model with second order actuator, $v_x = 18m/s$. Time delay 20 ms.

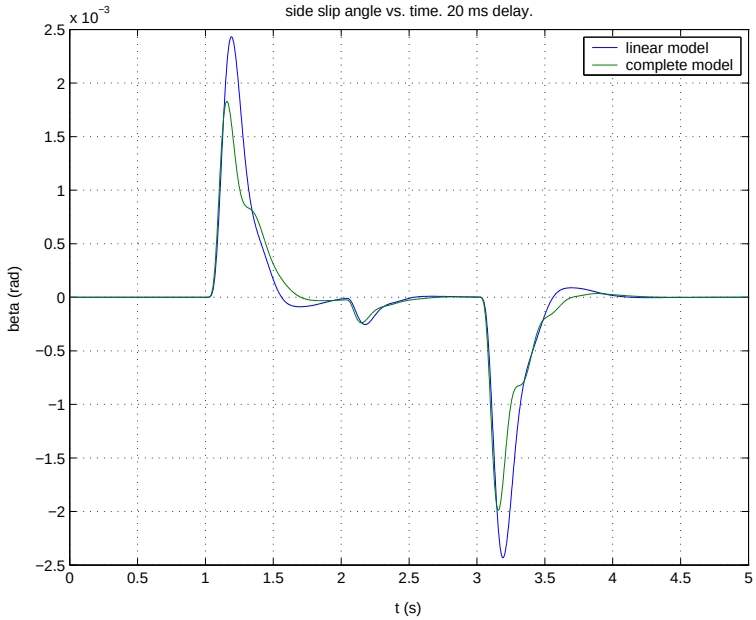

Figure 6.20: Simulation on model with second order actuator, $v_x = 18m/s$. Side slip angle β_r. Time delay 20 ms.

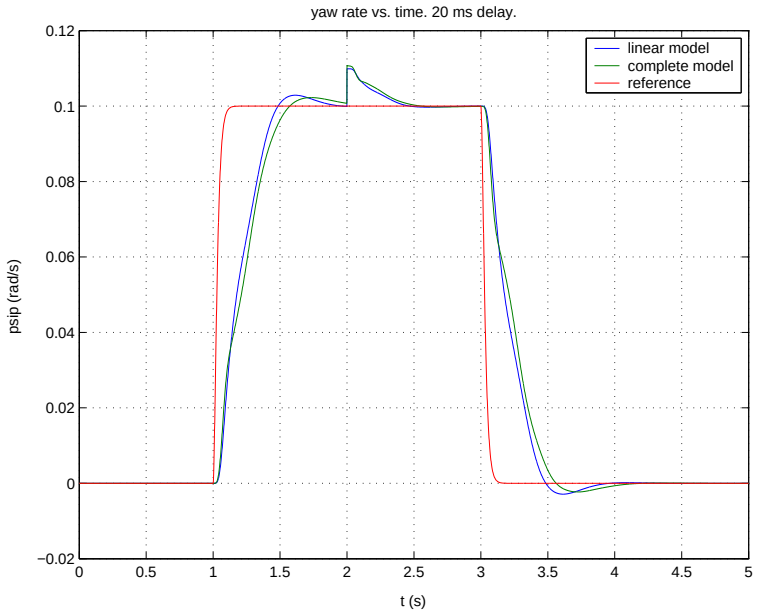

Figure 6.21: Simulation on model with second order actuator, $v_x = 14m/s$. Time delay 20 ms.

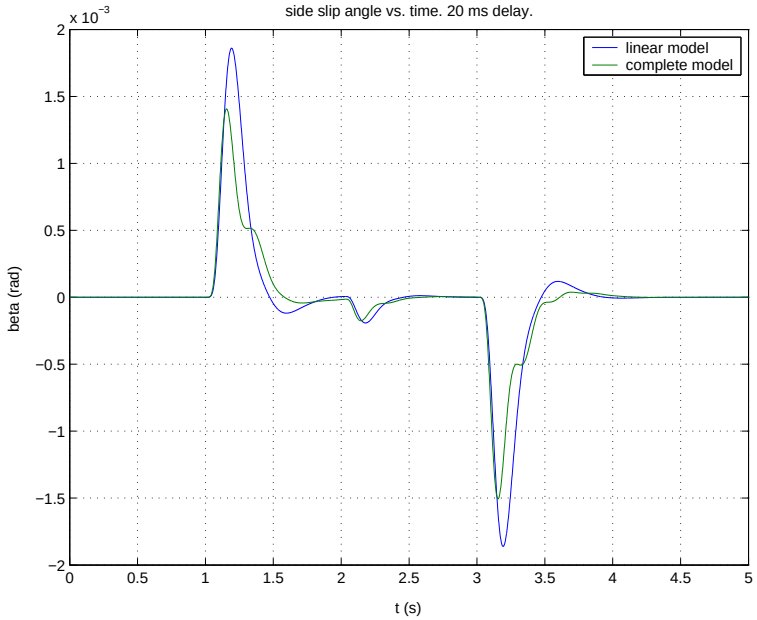

Figure 6.22: Simulation on model with second order actuator, $v_x = 14m/s$. Side slip angle β_r. Time delay 20 ms.

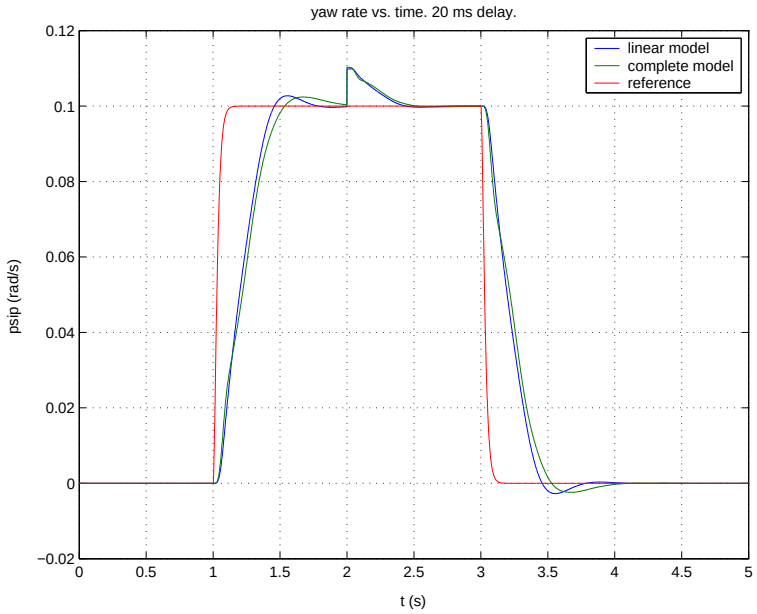

Figure 6.23: Simulation on model with second order actuator, $v_x = 10m/s$. Time delay 20 ms.

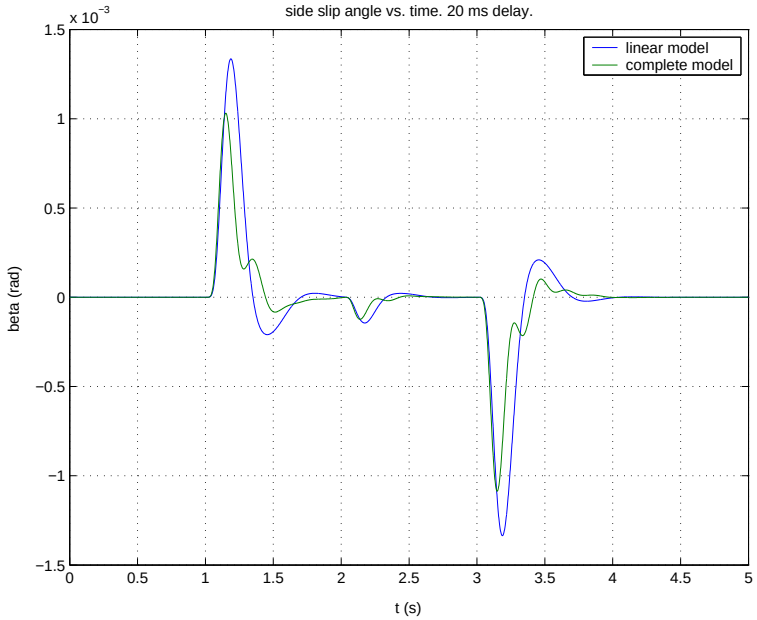

Figure 6.24: Simulation on model with second order actuator, $v_x = 10m/s$. Side slip angle β_r. Time delay 20 ms.

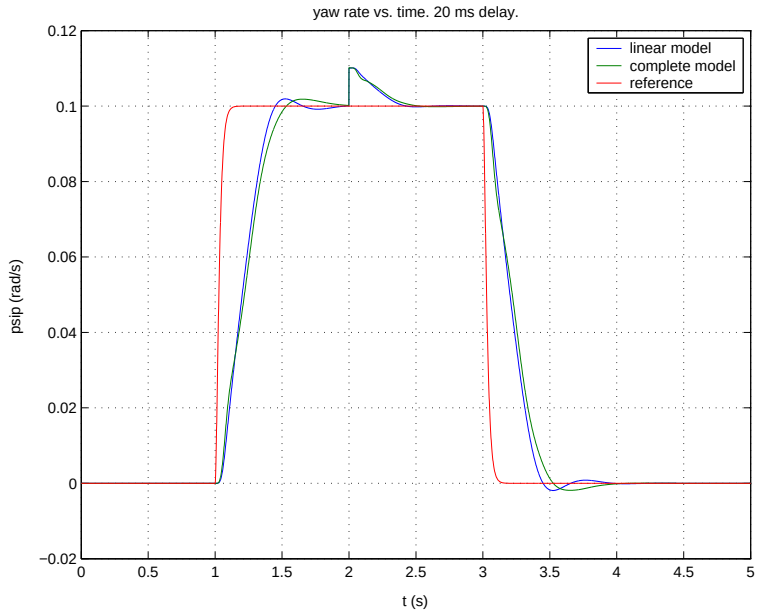

Figure 6.25: Simulation on model with second order actuator, $v_x = 8m/s$. Time delay 20 ms.

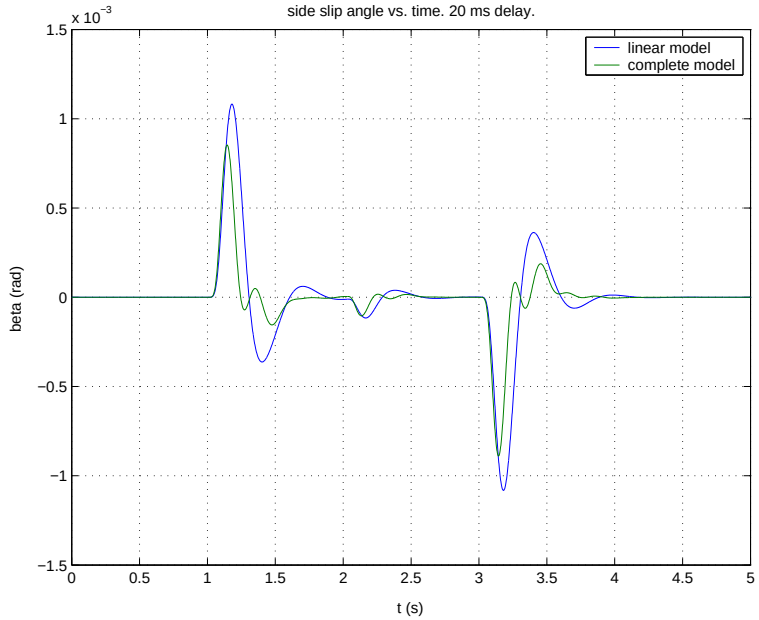

Figure 6.26: Simulation on model with second order actuator, $v_x = 8m/s$. Side slip angle β_r. Time delay 20 ms.

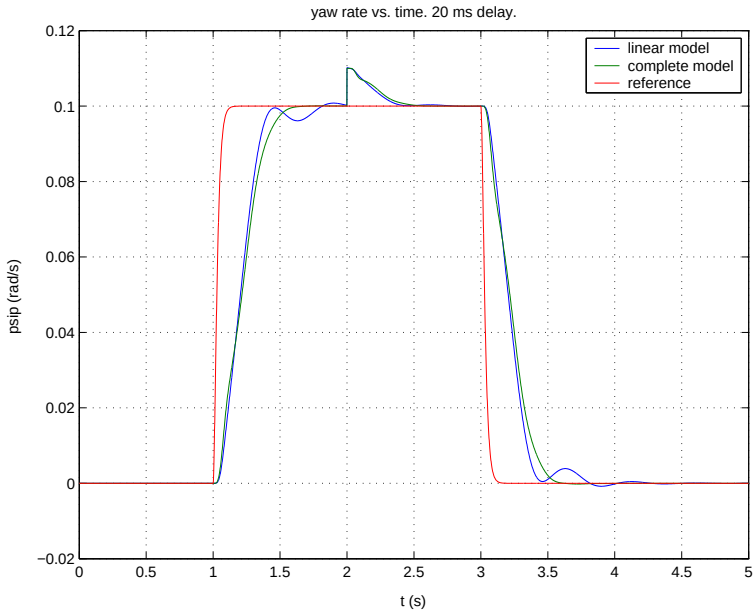

Figure 6.27: Simulation on model with second order actuator, $v_x = 5m/s$. Time delay 20 ms.

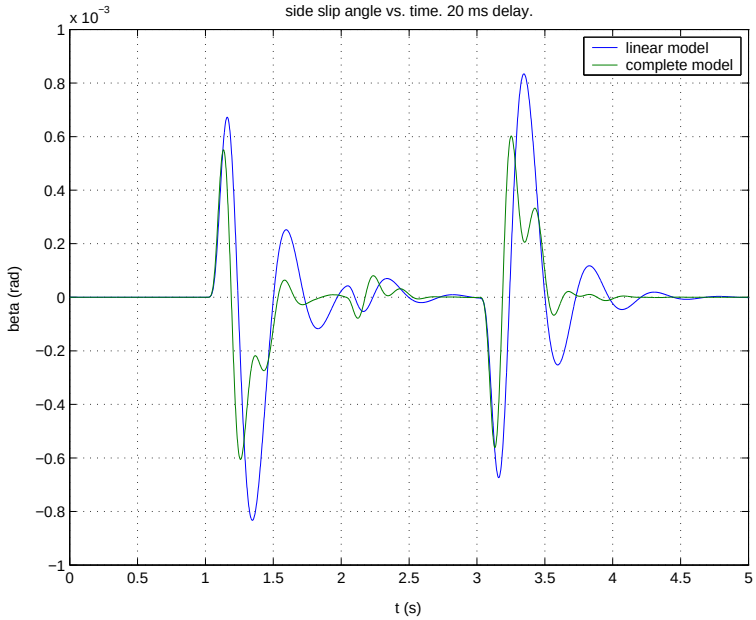

Figure 6.28: Simulation on model with second order actuator, $v_x = 5m/s$. Side slip angle β_r. Time delay 20 ms.

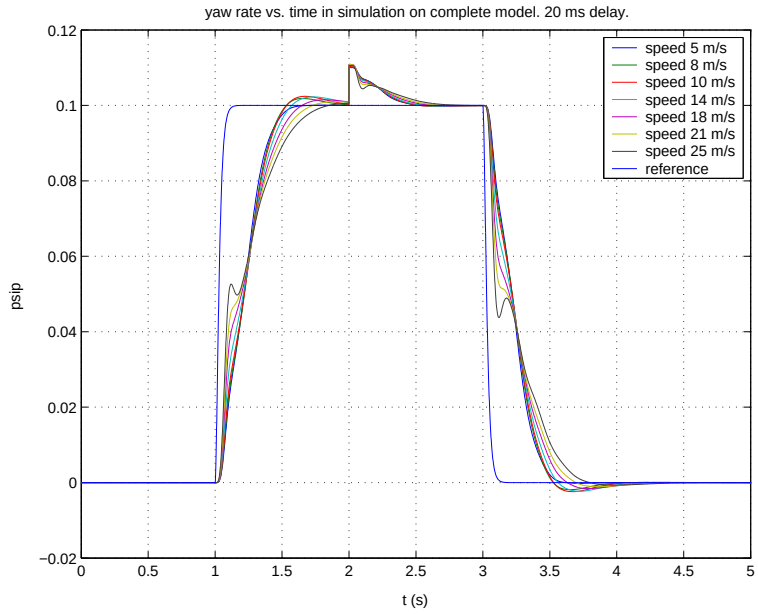

Figure 6.29: Simulation on model with second order actuator, for different speeds. Time delay 20 ms.

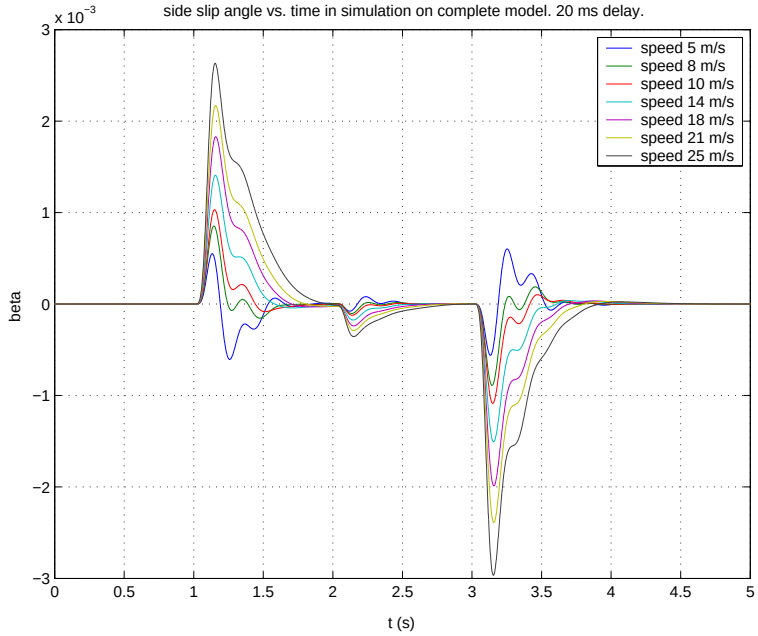

Figure 6.30: Simulation on model with second order actuator, for different speeds. Side slip angle β_r. Time delay 20 ms.

6.2 Keeping the Time Delay and Breaking the Second Loop

When one actuator fails, or, equivalently, when one of the loops is broken, the system should remain stable. Of course, control of both yaw rate and side slip angle, without using additional intervention such as, for example, braking, is then impossible. Figures 6.31 to 6.36 show the yaw rate and side slip angle when the rear actuator fails. In section 5.2 the performance of the controllers under a failure of one of the feedback loops was investigated. Despite a slight loss in phase margin, the performance of the loop in function remains the same. The side slip angle control remains stable but reference tracking is no longer possible. The steady state error after a couple of seconds is caused by the impulse disturbance applied after 2 seconds, and the absence of a closed loop integrator.

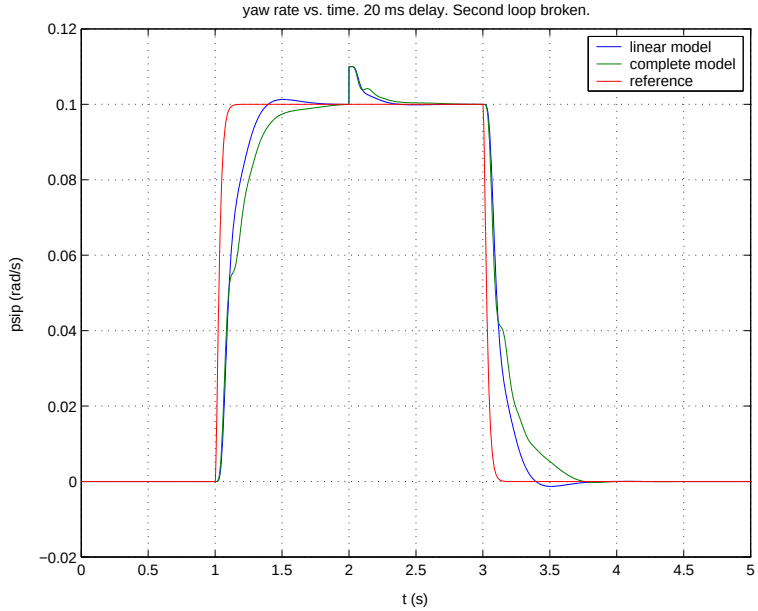

Figure 6.31: Simulation on model with second order actuator, $v_x = 25m/s$. Time delay 20 ms. Second loop broken.

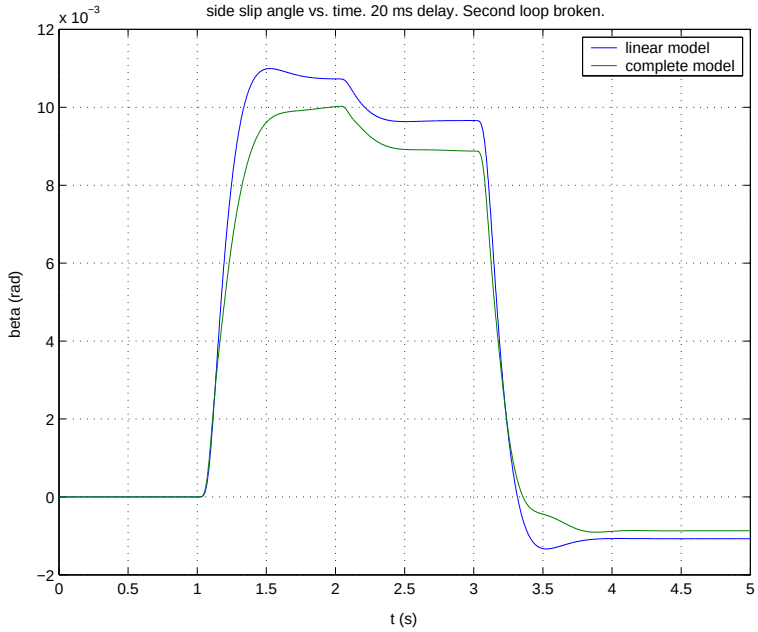

Figure 6.32: Simulation on model with second order actuator, $v_x = 25m/s$. Side slip angle β_r. Time delay 20 ms. Second loop broken.

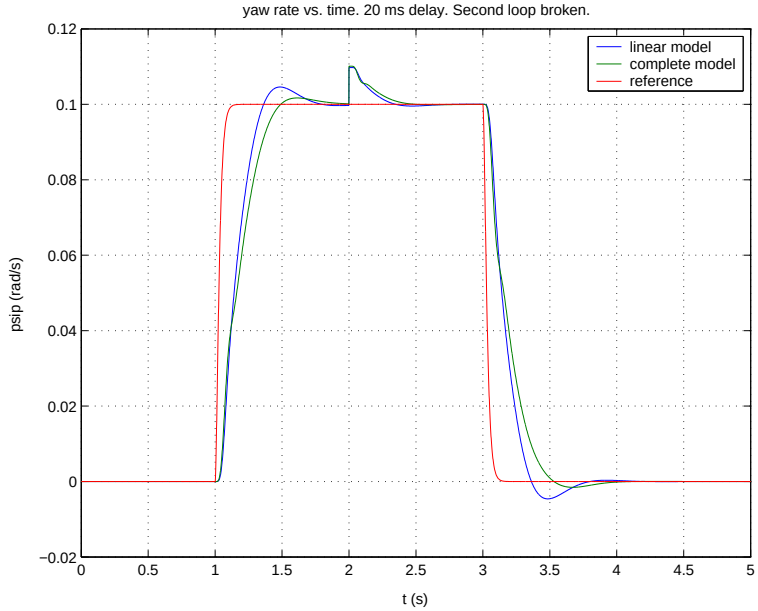

Figure 6.33: Simulation on model with second order actuator, $v_x = 18m/s$. Time delay 20 ms. Second loop broken.

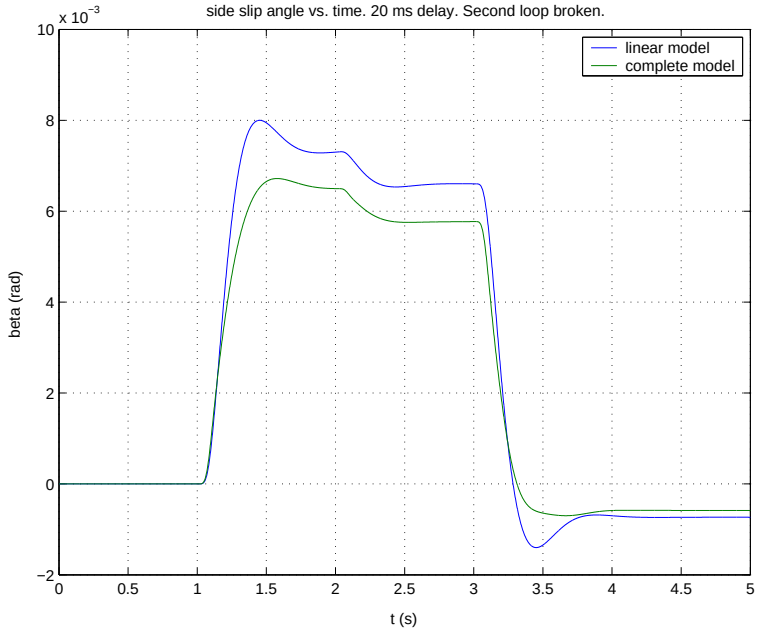

Figure 6.34: Simulation on model with second order actuator, $v_x = 18m/s$. Side slip angle β_r. Time delay 20 ms. Second loop broken.

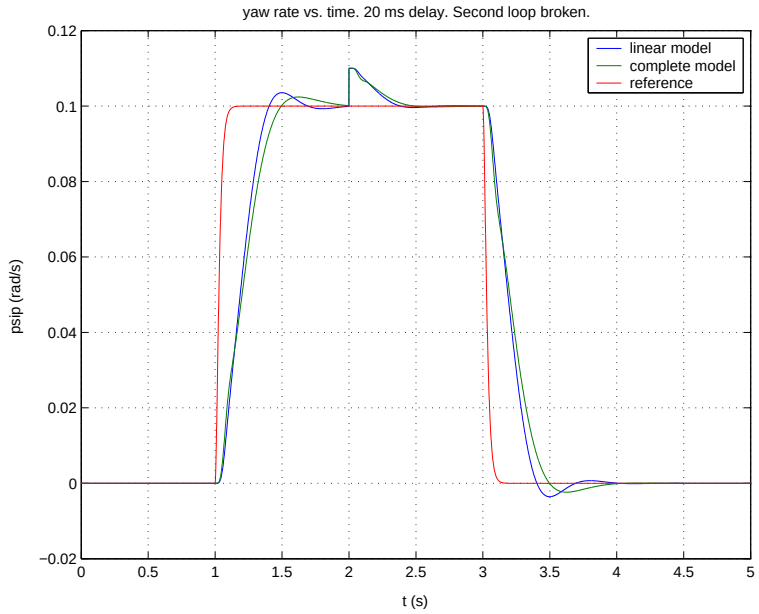

Figure 6.35: Simulation on model with second order actuator, $v_x = 10m/s$. Time delay 20 ms. Second loop broken.

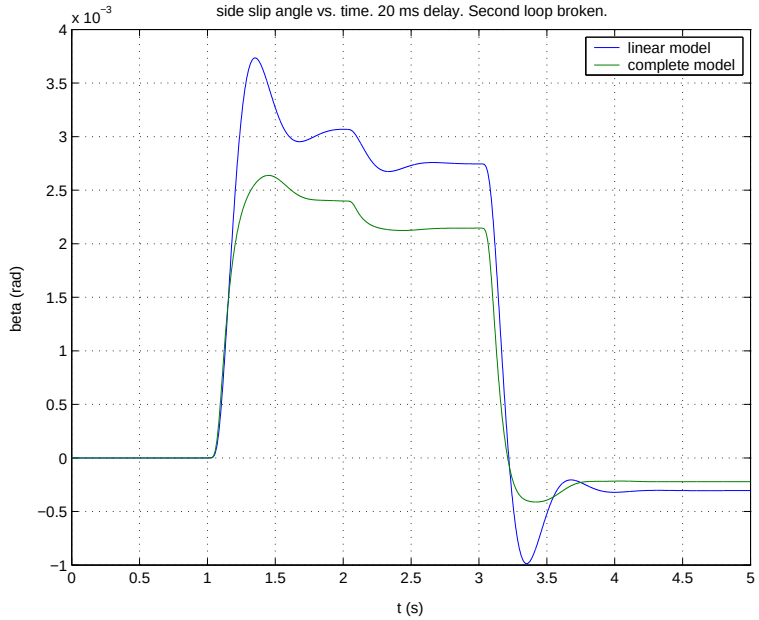

Figure 6.36: Simulation on model with second order actuator, $v_x = 10m/s$. Side slip angle β_r. Time delay 20 ms. Second loop broken.

7 Conclusions and Future Work

The main concept of this work has been the design of a diagonal feedback controller for yaw rate and side slip angle, using front and rear wheel steering. With the today existing decoupled design, there are obvious difficulties in obtaining a robust solution that can handle time delays as well as actuator and sensor failures or constraint hitting. Instead, coupling based on *Individual Channel Design* has been applied.

Of all approaches tested, the one presented in this report shows the best ability of fulfilling the specifications. It has a rather easy structure and the scheduling is quite straightforward. It can also easily be implemented as a PID-controller.

System integrity, or the performance of the closed-loop system under a failure of one of the feedback loops, has been studied. The theoretical requirements have been tested, by studying the pole placement of the channels, and by simulating on a car model.

Robustness to plant uncertainty is very important for the controller to work on a real plant. It can to some extent be verified in theory. This has been done by studying the structure function of the system, and by simulating on the car model. A 20 ms time delay has also been used to check the robustness. During the design it has been noticed that the plant dynamics show great variations with changing tyre characteristics, such as, for instance, the stiffness. This further increases the importance of having a robust solution.

The physical environment is very uncertain. Changes in the road surface and wind disturbances are always present. A rejection of those disturbances is important. An integrator is used in the controller to avoid steady state errors.

The specified bandwidth and phase margin have been obtained with the feedback design for the second channel. The first channel turned out to be quite ill behaved, and the bandwidth specification had to be relaxed for the first feedback loop. The lower bandwidth used will affect the performance in terms of the step and impulse response rise time. Despite the slower characteristics of the first loop, and the fact that the original specifications could not be completely fulfilled, feedback can still be used for both front and rear wheel steering.

A feedforward still remains to be designed. This can be done by using the general ideas about feedforward (some are presented in section 3.2). The feedforward used with the today existing feedback design, can possibly be applied. Furthermore, it should be investigated whether a change of the outputs would make design somewhat easier. The controllers also need to be implemented, and finally tested in the experimental vehicle.

A Matlab Commands

A.1 State Space Modelling

The linear car model that the controller design is based upon, is created with the following commands:

```
LV=1.673;
LH=3.085-1.673;
L=LV+LH;
J=5000;
m=2364;
vx=14;
TV=0.03; %time constants of the first order actuators
TH=0.03;
a = vx/(0.03*vx+0.5); %initialisation transient
b = J/LV/m/vx;
CV = 144000; %tyre stiffness
CH = 283000;
fg = 3; %closed loop bandwidth in Hz
wg=fg*2*pi;

A=[ 0,                              0,      LV/J,   -LH/J,      0,              0       ;
    1,                              0,      0,      -L/LV/m/vx, 0,              0       ;
   a*[-CV*(LV+J/LV/m)/vx,           CV,     -1,     0,          CV,             0]      ;
   a*[ CH*(LH-J/LV/m)/vx,           CH,     0,      -1,         0,              CH]     ;
    0,                              0,      0,      0,          -1/TV,          0       ;
    0,                              0,      0,      0,          0,              -1/TH   ;
  ];
B   = [0,0;0,0;0,0;0,0;1/TV,0;0,1/TH];
C   = [1,0,0,0,0,0; 0,1,0,0,0,0];
D   = zeros(2,2);

sys = ss(A,B,C,D);  %state space representation of plant with linear first order actuators.
Gbig= tf(sys);      %transfer function of sys.
PT1_front   = tf(1,[TV,1,0]); %first order actuator
PT1_rear    = tf(1,[TH,1,0]);

A1=[    0,                          0,      LV/J,   -LH/J       ;
        1,                          0,      0,      -L/LV/m/vx  ;
        a*[-CV*(LV+J/LV/m)/vx,      CV,     -1,     0]          ;
        a*[ CH*(LH-J/LV/m)/vx,      CH,     0,      -1]                 ;
   ];
B1  = [0,0;0,0;a*CV,0;0,a*CH];
C1  = [1,0,0,0;0,1,0,0];
sys1= ss(A1,B1,C1,D); %state space representation of plant with no actuators.
G   = tf(sys1);

Calt    = [1,0,0,0;-J/LV/m/vx,1,0,0];
sysalt  = ss(A1,B1,Calt,D); %plant with normal side slip angle (not rear axle) as output.

PT2_front   = tf([1],[0.012^2,0.612*0.012,1]); %second order actuator
PT2_rear    = tf([1],[0.0072^2,0.612*0.0072,1]);
G11 = G(1,1)*PT2_front; %second order actuator applied to the first channel.
G21 = G(2,1)*PT2_front;
G22 = G(2,2)*PT2_rear;  %second order actuator applied to the second channel.
G12 = G(1,2)*PT2_rear;

gamma   = minreal(G(1,2)*G(2,1)/G(1,1)/G(2,2)); %structure function of the plant.
H20     = tf(wg^2,[1,2*wg,wg^2]); %low pass filter with bandwidth wg.

G10 = minreal(G(1,1)*(1-gamma*H20));
```

A.2 An Iteration Step

An iteration could look as follows:

```
h2      = channeltf(Comp2,G22);
plant1  =   G11*(1-gamma*h2);
figure
bode(plant1,minreal(plant1,0.05)) %cancelling close poles and zeros,
                                  %and verifying that the open loop behaviour isn't changed.
plant1simple=minreal(plant1,0.05)
plant1simple=dcgain(plant1)*plant1simple/dcgain(plant1simple) %applying minreal requires
                                                              %correcting the dcgain.

function h=channeltf(k,g)
   h=minreal(k*g/(1+k*g));
   end;
```

The compensator *Comp1* will, together with *plant1*, represent the first channel. The root locus, open loop bode plot, closed loop step response and impulse response of the channel are then studied and the compensator modified to fit with the desired behaviour. This new compensator is then used for the second channel:

```
h1      = channeltf(Comp1,G1);
plant2  =   G22*(1-gamma*h1);
figure
bode(plant2,minreal(plant2,0.08)) %cancelling close poles and zeros,
                                  %and verifying that the open loop behaviour isn't changed.
plant2simple=minreal(plant2,0.08)
plant2simple=dcgain(plant2)*plant2simple/dcgain(plant2simple) %applying minreal requires
                                                              %correcting the dcgain.
```

Now, similarly, the second compensator, *Comp2*, is modified, and *plant1* is re-calculated, based on this new *Comp2*. This will give an updated first channel, and the iteration step is finished. This has to be repeated, until both channels get the desired behaviour.

A.3 Making a PID-controller

A.3.1 Converting into PID-parameters

The PID-controller can be re-written into the rational form, in which the design is initially done, as follows:

$$\begin{aligned} k_j &= K_P\left(1+\frac{sT_D}{1+sT}+\frac{1}{sT_I}\right) = \frac{K_P}{T_I}\cdot\frac{1+s\left(T_I+T\right)+s^2T_I\left(T_D+T\right)}{s\left(1+sT\right)} \\ &= \frac{K_P\left(T_D+T\right)}{T}\cdot\frac{s^2+s\frac{T_I+T}{T_I(T_D+T)}+\frac{1}{T_I(T_D+T)}}{s\left(s+\frac{1}{T}\right)} = K\frac{\left(s-z_j\right)\left(s-z_j^*\right)}{s\left(s+\frac{1}{T}\right)} \\ &= K\frac{s^2-2Re\{z_j\}+z_jz_j^*}{s\left(s+\frac{1}{T}\right)} \end{aligned} \tag{A.1}$$

This would give the PID-parameters in terms of T, the complex zero pair z_j and z_j^*, and gain K:

$$T_I = -\frac{2Re\{z_j\}}{z_j z_j^*} - T \tag{A.2}$$

$$T_D = \frac{1}{T_I} \cdot \frac{1}{z_j z_j^*} - T \tag{A.3}$$

$$K_P = K\frac{T}{T_D + T} \tag{A.4}$$

A.3.2 Scheduling with respect to speed

The controller zero is placed right on the lightly damped pole of the plant. The complex zero calculation is done with the following function, where the inputs are the car parameters and the current speed.

```
function z=makezero(LV,LH,m,J,CV,CH,vx)

L=LV+LH; a = vx/(0.03*vx+0.5);
pss_f=-CV*(LV+J/(LV*m))/vx;
pss_r=CH*(LH-J/(LV*m))/vx;
A1pol=[ 1;
        2*a;
        a^2+a*CH*L/(LV*m*vx)-(a*pss_f*LV/J)+a*pss_r*LH/J;
        a^2*CH*L/(LV*m*vx)-(a*CV*LV/J)-(a^2*pss_f*LV/J)+a^2*pss_r*LH/J+a*CH*LH/J;
        -a^2*CV*LV/J-a^2*CH*pss_f*L/(LV*m*vx)*LV/J+a^2*CV*pss_r*L/(LV*m*vx)*LV/J+a^2*CH*LH/J
        ]'; %characteristic polynomial of the state matrix A.

poles=roots(A1pol); %poles of the plant.

place_of_pole=find(real(poles)==max(real(poles))); %finds the lightly damped pole.
z=poles(place_of_pole(1));
z=real(z)+abs(imag(z))*i; %returns the lightly damped pole with positive imaginary part.
```

The compensator gains, K_1 and K_2, are calculated as follows:

```
function [Gain_Comp1,GainComp2] = makegain(LV,LH,m,J,CV,CH,vx)

L=LV+LH;
a = vx/(0.03*vx+0.5);
    A1=[    0,                                  0,      LV/J,   -LH/J;
    1,                                  0,      0,      -L/LV/m/vx;
   a*[-CV*(LV+J/LV/m)/vx,       CV,     -1, 0];
   a*[ CH*(LH-J/LV/m)/vx,       CH,     0,      -1];
  ];
B1 = [0,0;0,0;a*CV,0;0,a*CH];
C1 = [1,0,0,0;0,1,0,0];
D = zeros(2,2);
sys1 = ss(A1,B1,C1,D);
G = tf(sys1); %system transfer function
G11 = G(1,1)*tf([1],[0.012^2,0.612*0.012,1]); %second order actuator applied to channel 1.
G22 = G(2,2)*tf([1],[0.0072^2,0.612*0.0072,1]); %second order actuator applied to channel 2.
gamma = minreal(G(1,2)*G(2,1)/G(1,1)/G(2,2));

zero = makezero(LV,LH,m,J,CV,CH,vx); %finds the complex zero for speed vx.
```

```
Gain_Comp1=abs(evalfr(zpk([zero zero'],[0 -80],1)*G11*(1-gamma),i*5))^-1;
            %gain of first compensator.
Comp1=zpk([zero zero'],[0 -80],Gain_Comp1);
h1=channeltf(Comp1,G11));
Gain_Comp2=-abs(evalfr(zpk([zero zero'],[0 -80],1)*G22*(1-gamma*h1,i*18))^-1;
            %gain of second compensator.
Comp2=zpk([zero zero'],[0 -80],Gain_Comp2);
```

Since the gain K and zero z_j are known, the PID-parameters can easily be calculated using equations A.2, A.3 and A.4. During simulation, the parameters are calculated frequently, for example at every sampling instant.

A.3.3 Discretising the controller

The controllers can be discretised in different ways. Euler's method, backward difference and Tustin's approximation are some examples and are explained in [Åström]. The assumption is that the continuous-time controller is given as a transfer function. The discrete pulse-transfer function $H(z)$ is obtained by replacing the argument s in $G(s)$ by s', where s' is a function of the discrete z-variable and $H(z) = G(s')$.

- Tustin's approximation
$$s' = \frac{2}{h} \cdot \frac{z-1}{z+1} \tag{A.5}$$
- Backward difference
$$s' = \frac{z-1}{zh} \tag{A.6}$$
- Euler's method
$$s' = \frac{z-1}{h} \tag{A.7}$$

References

[Glad] Torkel Glad, Lennart Ljung, Reglerteknik, Grundläggande teori, 1997 Studentlitteratur

[Glad2] Torkel Glad, Lennart Ljung, Reglerteori, Flervariabla och olinjära metoder, 1997 Studentlitteratur

[Hayes] Monson H. Hayes, Statistical Digital Signal Processing and Modeling, John Wiley & Sons 1996

[Horowitz] Isaac M. Horowitz, Synthesis of Feedback Systems, Academic Press 1963

[Kalkkuhl] Jens Kalkkuhl, Individual Channel Design - Ein Werkzeug zur Analyse und Synthese Robuster Mehrgrössenregelungen im Frequenzbereich, Daimler Benz 1997

[Kiencke] U. Kiencke, L. Nielsen, Automotive Control Systems, For Engine, Driveline, and Vehicle, 2000 Springer

[Kleinschrodt] Thomas Kleinschrodt, Four Wheel Steering Considering the Nonlinear Wheel Slip - An Anti Windup Problem, Daimler Chrysler 2001

[Leithead,O'Reilly] W.E. Leithead,J. O'Reilly, Performance issues in the individual channel design of 2-input 2-output systems, Int. J. Control 1991-1992

[Maciejowski] J.M. Maciejowski, Multivariable Feedback Design, 1989 Addison-Wesley

[Niethammer] Marc Niethammer, Reglerentwurf für ein Fahrzeug mit lenkbarer Vorder- und Hinterachse, Daimler Chrysler 2000

[Nieuwstadt] Michiel J. van Nieuwstadt, Trajectory Generation for Nonlinear Control Systems, California Institute of Technology 1997

[Årzen] Karl-Erik Årzen, Real-Time Control Systems, Dept. of Automatic Control, Lund Institute of Technology 2001

[Åström] K.J. Åström, Björn Wittenmark, Computer Controlled Systems, Theory and Design, 3rd ed, 1997 Prentice Hall